Austrian Journal of Earth Sciences | Volume 107/2 | 37 - 59 | Vienna | 2014

Small- to meso - scale brittle rock structures and the estimation of "paleostress" axes – A case study from the Koralm region (Styria/Carinthia)

Franz-Josef BROSCH[1)] & Gerald PISCHINGER[1)2)*)]

KEYWORDS

paleostress analysis
brittle tectonics
Koralm Tunnel
Florianer beds
Eastern Alps
Badenian
Koralpe

[1)] Institute of Applied Geosciences, TU Graz, Rechbauerstraße 12, A-8010 Graz, Austria;

[2)] Geoconsult ZT GmbH, Hölzlstraße 5, A-5071 Wals bei Salzburg, Austria;

[*)] Corresponding author, gerald.pischinger@tugraz.at

Abstract

Mapping of fault slip data and the consecutive estimation of paleostress orientations are routine procedures during structural geological investigation. In addition, there are various other small- to mesoscale features of brittle deformation which are frequently neither mapped nor routinely used for paleostress analysis. In this paper we present such data, i.e. conjugate shear fractures, faulting related secondary fractures, tensile/extensional fractures, veins, low angle shears and listric faults, from the Koralpe, Eastern Alps. Paleostress orientations are determined with the help of stereographic projection techniques and compared to the results of published fault slip data and fault slip data gathered during tunnelling of the Koralm Tunnel in the Badenian Florianer beds of the western Styrian Basin. The analysed data yield paleostress axes which may be attributed to the three Andersonian fault types with similar orientations as the ones achieved by fault slip analysis. Yet, a reliable (relative) timing of the different tectonic events is not possible on the basis of the structures analysed and time constraints from the surrounding basins are limited to Ottnangium till Sarmatium. Hence, a calibration for possible Paleogene brittle tectonic event(s) is not possible at present. Data attributable to normal faulting can be summarized to three directions of extension (SW-NE, W-E and NNW-SSE). SW-NE directed extension dominates the area near to the Lavanttal fault zone, indicating the opening direction of the Lavanttal Basin. More pronounced scatter of extension direction characterizes the central Koralpe, σ_3 directions indicate W-E, NW-SE and NE-SW extension respectively. W-E directed extension (fluctuating between WSW-ENE and WNW-ESE) dominates the eastern margin towards the Styrian Basin. "Strike slip" data can be summarized to represent two events, with interchanging orientation of the σ_1 and the σ_3 axes. The vicinity of the Lavanttal fault zone is characterized by N-S to NW-SE directed compression axis. N-S to NNE-SSW directed σ_1 dominates the central area of the Koralpe. The eastern margin yields predominating W-E to WNW-ESE directed, and single N-S directed σ_1 axes. Moderate reverse faultings in WSW-ENE to WNW-ESE direction is confirmed. Yet similar structures are not known from the Styrian Basin and therefore age constraints are missing. Similarity of σ_1 orientations to some of the strike slip data indicates a relationship to strike slip tectonics.

Die Aufnahme von Störungsflächen-/ Striemungsdaten und die Ermittlung der dazugehörigen Paläospannungsorientierungen sind geologischen Standardtechniken. Dem gegenüber gibt es zahlreiche durch spröde Deformation entstandene Strukturen, die meist nicht kartiert und dementsprechend auch nicht routinemäßig für Paläospannungsanalysen verwendet werden. Anhand von konjugierten Scherbrüchen, Scherflächengeometrien in Scherzonen, Klüften (im Sinne von reinen Trennbrüchen), Fiederklüften, „low angle shears" und listrischen Störungsflächen aus dem Bereich der Koralpe wurde mit der Hilfe von Lagekugeltechniken die dazugehörigen Paläospannungsrichtungen ermittelt und mit publizierten Ergebnissen von Störungsflächen-/ Striemungsanalysen aus dem Bereich der Koralpe verglichen. Störungsflächendaten die im Zuge des Vortriebs des Koralmtunnels in den badenischen Florianer Schichten des westlichen Steirischen Beckens gewonnen wurden liefern weitere Anhaltspunkte für die zeitliche Zuordnung der Daten aus dem Kristallin. Eine relative zeitliche Einordnung der neuen Daten aus dem Kristallin ist auf Basis der Daten allein nicht möglich und die Sedimentationgeschichte der angrenzenden Becken ist auf den Zeitraum Ottnangium bis Sarmatium beschränkt, was die Interpretation der Daten auch in Bezug auf mögliche paläogene Ereignisse erschwert. An den Strukturen die sich als das Resultat von Abschiebungstektonik interpretieren lassen, können drei Extensionsrichtungen unterschieden werden: SW-NE, W-E und NNW-SSE. SW-NE gerichtete Extensionstektonik dominiert im Nahfeld der Lavanttaler Störungszone und deutet die Öffnungsrichtung des Lavanttaler Beckens an. Die Daten aus dem zentralen Teil der Koralpe zeigen eine ausgeprägte Streuung und es lässt sich Extension in W-E, NW-SE und NE-SW Richtung unterscheiden.W-E gerichtete, zwischen WSW-ENE und WNW-ESE streuende Extension dominiert den östlichen Teil des Untersuchungsgebiets, am Rande des Steirischen Beckens. Weiters lassen sich zwei Gruppen von Strukturen unterscheiden, die als Seitenverschiebungsstrukturen interpretiert werden können. Sie unterscheiden sich durch einen Positionstausch der größten und der kleinsten Hauptnormalspannung. Das Nahfeld der Lavanttalstörung wird von N-S bis NW-SE gerichteten Kompressionsachse dominiert. N-S bis NNE-SSW gerichtete Kompression dominiert die zentrale Koralpe. Am Ostrand der Koralpe wurden überwiegend W-E bis WNW-ESE gerichtete Kompressionsachsen ermittelt. Einzelne Strukturen indizieren eine

N-S gerichtete σ_1 Achse. Schwach ausgeprägte Kompressionstektonik mit WSW-ENE bis WNW-ESE gerichtetem σ_1 und etwa vertikalem σ_3 wird durch die Geländedaten bestätigt. Aus dem Steirischen Becken sind solche Strukturen nicht bekannt und eine zeitliche Zuordnung der Kompressionsstrukturen aus dem Kristallin ist daher nicht möglich. Eine mögliche Interpretation wäre aufgrund der ähnlichen Orientierung von σ_1 die Zugehörigkeit dieser Daten zu den dokumentierten Seitenverschiebungsereignissen.

1. Introduction

Brittle fracture results from a deformation process, which is in the first place pressure-dependent and involves volume increase due to cracking, fracturing and frictional sliding, including detrition of particles. In the ideal case these phenomena are restricted to particular planes. Mandl (2000) defines a macroscopic deformation process as “brittle”, if it is rate-independent and strain-softening in the post-peak region. The involved failure modes and sequences (e.g. Lajtai and Lajtai, 1974), led to the current geological terminology comprising joints, shears, faults, and their sub-divisions (e.g. Pollard and Aydin, 1988; Mandl, 2000; Twiss and Moores, 2007).

Kinematic indicators on fault slip planes (as, e.g., scratches, ridge-in-grove striae, fibre crystals, mineral growth in extensional gashes, linear imprints or gouge material accumulations) are most useful tools in the reconstruction of relative displacements along these discontinuities (e.g. Fleuty and Weaver, 1975; Scholz and Engelder, 1976; Engelder and Scholz, 1976; Petit, 1987; Doblas et al., 1997; Doblas, 1998; Fry, 1999). Several methods for both manual and computerized 2D – 3D extraction of principal stress directions and “paleostress” tensors from fault slip data have been developed during the last decades (see discussion and references in Etchecopar et al., 1981; Angelier, 1989, 1994; Meschede, 1994; Celerier, 1999; Ortner et al., 2002). However, pre-assumptions of initial approaches have not remained undoubted (e.g., Schrader, 1994, 1999).

Additional to fault slip data, other features of brittle deformation (mainly arrays of fractures, see Beach, 1975; Hancock, 1985; Hancock et al., 1987; Dunne and Hancock, 1994; Srivastava, 2000; Blenkinsop, 2008) may serve in unravelling brittle tectonic history. These structural associations are found abundantly in the field, even in bad outcrop conditions. However, the interest into most of these structures has not been strong enough to evoke the development of specific, generally available software tools for straightforward kinematic analysis of such data. Useful introductory and advanced instructions for the use of hemispherical projection techniques and their application by simple trigonometric calculations are found in several textbooks on structural geology and rock engineering (e.g., Ragan, 2009; John and Deutsch, 1974; Goodman, 1976, 1989; Quade, 1984; Priest, 1985, 1993; Wallbrecher, 1986; Meschede, 1994; Lisle and Leyshon, 2004; Wyllie and Mah, 2004).

Some of the more common brittle structure associations and their usage in simple kinematic and stress axes interpretation are outlined below. The text intends to show - by a few examples - the potentials of simple “Schmidt-net” constructions and the ambiguity of interpretation, too. The estimated axes are discussed within the framework of published stress axes estimates (Fodor et al., 2008; Pischinger et al., 2008; Reischenbacher and Sachsenhofer, 2013). Further constraints come from unpublished fault-slip data documented during the excavation of the Koralm Tunnel (lot KAT1) in Badenian (Middle Miocene) sediments of the Styrian Basin.

The analysis of fault slip data is not discussed further in the present paper, as it follows the commonly accepted and published methods (e.g. Petit, 1987; Angelier, 1994; Meschede, 1994; Doblas, 1998; Fossen, 2010). In the text below the term “paleostress” is used under quotes as a reminder that the stress axes are reconstructed from observed traces of displacements.

Case studies come from mapping campaigns for a major subsurface infrastructure project in southeastern Austria; example locations are referenced to the Austrian BMN M34 coordinate system. Due to inaccuracies in the outcrop localization on the mapping sheets (1:5.000), outcrop-grouping, and changing of reference systems, an error not in excess of few tens of meters may occur. The input data for the paleostress analyses are listed in Table 1 (Online Appendix).

2. Geological setting

The project area is situated within the polymetamorphic rocks of the Koralpe mountain range in southeastern Austria (Fig. 1), and belongs to the Austroalpine basement units. The Koralpe block is characterized by a linear western mountain front along the Lavanttal Basin, attributed to the Lavanttal fault (Popotnig et al., 2007). The southern margin follows the Drau (Drava) valley, its linearity proposes a fault controlled setting, too. In the east the contact to the sediments of the Styrian Basin is undulating, indicative of neotectonic quiescence.

To the north the Koralpe is connected to the Stub- and Gleinalpe by a zone of low relief caused by prominent paleosurfaces, all belonging to the so called “Styrian block” (Wagner, 2010). In places gravel deposits are preserved on top of these paleosurfaces. The age of these deposits is not directly constrained by biostratigraphy. Beck-Mannagetta (1980) assigned a (questionable) Pliocene age to these deposits, whereas Thiedig and Weissenbach (1975) correlated them to deposits in the area of the Saualpe and other Carinthian regions and proposed a Middle Eocene to Middle Miocene age for these remnants of ter-

Figure 1: Geological map of the Koralpe and adjacent areas, including the main faults active during the Miocene and the main drainage pattern in this region. Black rectangle indicates the project area. Geology compiled from Beck-Mannagetta, 1952; Weissenbach, 1978a; Weissenbach, 1978b; Becker, 1979; Beck-Mannagetta, 1980; Kröll, 1988; Beck-Mannagetta et al., 1991; Egger et al., 1999; Joanneum Research and GIS-STMK, 1999; Strauss et al., 2001; Beck-Mannagetta and Stingl, 2002, mappings by 3G ZT GmbH (courtesy of ÖBB Infrastruktur Bau GmbH) and own mappings. Digital elevation data are from space shuttle radar topographic mission (SRTM, 96.36 m resolution, http://srtm.csi.cgiar.org/).

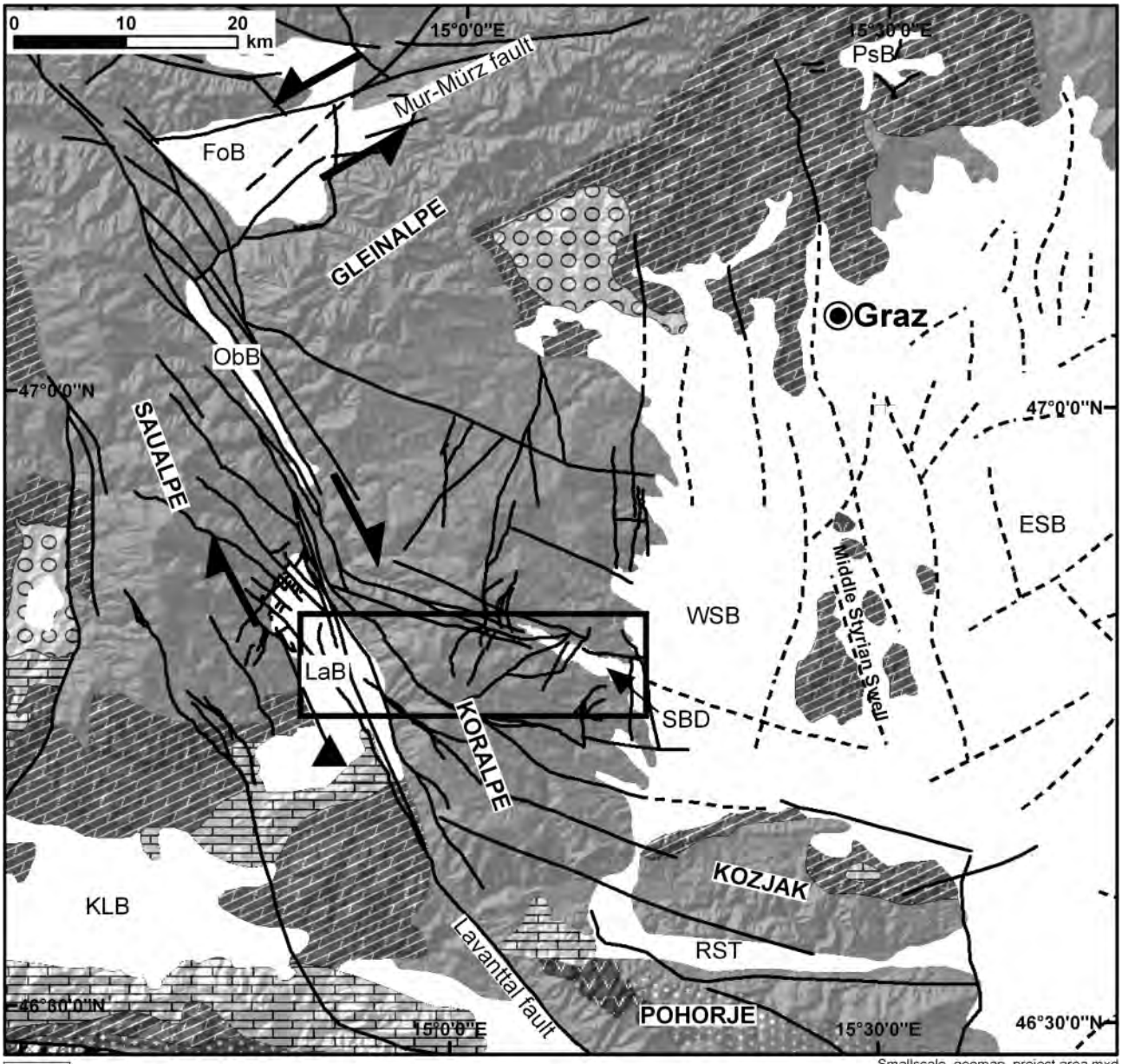

Neogene sediments
Volcanic rocks (Miocene-Pliocene)
Plutonic rocks (Miocene)
Plutonic rocks (Oligocene)
Gosau Group (U.Cretaceous - Eocene)
Austroalpine Cover (Permian - Mesozoic)
Graywacke zone
Graz Paleozoic/Gurktal Nappe system
Central Austroalpine basement
South Alpine units
Basalt pipe (Badenian)
Fault
Fault (in basin floor)

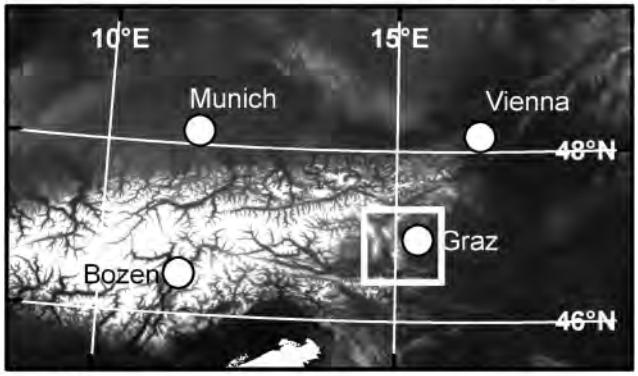

Abbreviations:

FoB	Fohnsdorf Basin	LaB	Lavanttal Basin
ObB	Obdach Basin	KLB	Klagenfurt Basin
PsB	Passail Basin	RST	Ribnica-Selnica Trough
WSB	Western Styrian Basin		
ESB	Eastern Styrian Basin		
SBD	Schwanberg block debris		

restrial sedimentary conditions. In the eastern region of the Koralpe a block debris basin of Badenian age (Nebert, 1989; Pischinger et al., 2008) is preserved several hundred meters above the Styrian Basin. In the Lavanttal Basin Miocene sedimentation started in the Karpartian, lasting up to the Middle Pannonian (Reischenbacher, 2008; Pischinger at al., 2008, and references therein). In the Styrian Basin sedimentation started in the Ottnangian. Within the Western Styrian Basin, Miocene sedimentation ends for the larger part in the Badenian, and Lower Sarmatian sediments are only preserved in places (Reischenbacher, 2008; Pischinger et al., 2008, and references therein).

The Koralpe itself is characterised lithologically by mica schists, paragneisses, eclogites and mylonites. For a discussion of the metamorphic evolution refer, e.g., to Kurz et al. (2002). Structurally, the Koralpe is dominated by large scale, open fold structures with WNW-ESE trending fold axes (e.g. Putz et al., 2006). Low temperature geochronology shows that the northern Koralpe and the Gleinalpe had already cooled below 200°C during the Late Cretaceous (Hejl, 1997, 1998). Formation of the Gosau basin of Kainach at the NE margin of the Koralpe is regarded as a consequence of uplift and exhumation during this time (Ebner and Rantitsch, 2000). Generally, the apatite fission track ages within the Koralpe become younger from north to south, ranging from 52 to 31 Ma (Wölfler et al., 2011). It can be concluded that exhumation was largely terminated within the Paleogene and topography was characterized by low relief (Dunkl et al., 2005). The thermochronological evolution constrains that the Koralpe was subjected to brittle tectonic conditions throughout the Paleogene and Neogene. However, Paleogene sediments are only sparsely recorded in this part of the Eastern Alps, the nearest occurrence is the Krappfeld Eocene at the western side of the Saualpe (Kurz and Fritz, 2003), and stratigraphic constraints for the brittle tectonic evolution of the Koralpe from the surrounding basins are restricted to a sedimentary history from the Lower Miocene onwards (Fig. 2). Within the Lavanttal fault itself distinct faulting events are constrained by thermochronology from the Miocene up to the Pliocene (Kurz et al., 2011).

Brittle deformation of this area has sparsely been discussed in literature before the start of site investigations for the Koralm Tunnel in the late 1990ies. Neubauer (1991) had described three generations of steeply inclined fissures and the associated mineral parageneses. From the latter, indicating a decline in metamorphic conditions, he deduced three possible phases of extension. The oldest two fissure generations indicate W-E directed extension, followed by younger extension in SSW-NNE direction. These fissures were described to postdate the Alpidic peak metamorphism.

Vanek et al. (2001) broke down the history of brittle deformations in the Koralm rock mass from the analysis of drill cores, deducing sustained E-W directed extension during lateral extrusion of the Eastern Alps (Ratschbacher et al., 1991), followed by E-W compression and N-S extension, respectively. This far-field reorientation of the stress field is timed as Late Miocene, based on the work of Peresson and Decker (1997) and Reinecker and Lenhardt (1999). This event is also indicated by data from the Pohorje pluton (Fodor et al., 2008). However, compressional tectonic features have so far not been described from the Styrian Basin (see Wagner, 2010), in contrast to the Pannonian Basin s.s. (e.g. Fodor et al., 1999; Bada et al., 2007). Fault-slip data from Badenian, Upper Sarmatian and Pliocene sediments (east of the Middle Styrian Swell) indicate young extensional tectonics within the Styrian Basin (Wagner, 2010). This is supported by burial ages of sediments (1.56 Ma ± 1.11) entrapped within Devonian rocks from the Paleozoic of Graz (Wagner, 2010).

A comprehensive scheme of the tectonic evolution of the Koralpe during the Miocene from 18 Ma (Ottnangian, Early Miocene) up to the Pliocene was proposed by Pischinger et al. (2008), based on fault slip analysis and constraints from the surrounding sedimentary basins. The scheme comprises four main stages of tectonic evolution (D1 to D4, Fig. 2): D1-1 is characterised by strike slip tectonics caused by NNW-SSE compression and the formation/activation of WNW-ESE striking, dextral faults. In extensional domains these faults probably widened (D1-2) and block debris basins formed. Further W-E extension (Early Badenian) caused tilting of basement blocks and the formation of horst and graben structures within the Styrian Basin along N-S trending faults respectively. The separation of the Eastern and the Western Styrian Basin is attributed to these tectonic events. D3 is characterised by NE-SW directed compression and caused reactivation of strike slip faults in the opposite direction (D3-1). Simultaneously NW-SE directed extension caused normal displacement along N-trending faults (D3-2) and further subsidence within the Styrian and the Lavanttal Basins. During the late Pannonian the entire Styrian Basin became an erosional domain. Compressional structures within the Koralpe indicating W-E compression (D4) may be related to this event. However, compressional structures have only been reported from the Eastern Styrian Basin (Peresson and Decker, 1996).

The sequence of paleostress orientations proposed by Pischinger et al. (2008) was adopted and refined by Reischenbacher (2008) and Reischenbacher and Sachsenhofer (2013) for brittle structures of the Lavanttal Basin and its direct vicinity (Fig. 2). Fault-slip data indicating W-E directed compression are restricted to the eastern basin margin. Additionally, Reischenbacher and Sachsenhofer (2013) found data supporting young (Pleistocene?) strike slip kinematics along the basin margin and proposed a weakly constrained “D5” event. In-situ stress measurements from the realm of the Koralpe are compatible with the respective orientation of the maximum horizontal stress (Fig. 2, Goricki and Harer, 2004). Sedimentation along basins of the Noric Depression (e.g. Fohnsdorf, Trofaiach, Leoben, Parschlug, and Aflenz basins) is restricted to a single stage sedimentary history from the Karpatian up to the middle Badenian (Reischenbacher and Sachsenhofer, 2013). Only the Fohnsdorf Basin was subjected to a second stage, linked to half-graben formation from the middle to the late Badenian

(Strauss et al., 2001).

South of the Koralpe, Fodor et al. (2008) were able to deduce three tectonic phases for the Pohorje mountain range from the Miocene up to the Quaternary (Fig. 2). Phase 1 is characterized by a W-E directed extensional regime from the Early Miocene throughout the Middle Miocene, constrained by dykes and normal faults. Around the late Sarmatian and the early Pannonian a strike-slip stress field with a NE to E trending compression axis is discernable (phase 2, Fodor et al., 2008). A third phase is characterised by strike-slip and reverse faults, yielding a compression axis between NNW-SSE and NNE-SSW, lasting from the Late Miocene up to the Quaternary. These orientations are compatible with the orientation of the maximum horizontal stress as derived from in-situ stress measurements (Fig. 2, Goricki and Harer, 2004). Further to the west, within the Klagenfurt Basin sedimentation did not start before the the Sarmatian, which is clearly later than in the other basins (Fig. 2, Reischenbacher and Sachsenhofer, 2013). According to Nemes et al. (1997) the evolution of this flexural basin is connected to transpressive dextral strike-slip deformation along the Periadriatic Fault and the NW directed overthrust of the Karawanken Mountains.

3. Structural associations

3.1 Conjugate shear fractures

The idea of conjugate shear fractures (Fig. 3 a, Fig. 4, see discussion in chapter 5.1) is based on the Coulomb fracture criterion which can be demonstrated graphically in a Mohr Circle diagram and has early been shown in experiments by Riedel (1929). The well-known construction of (principal) stress axes for this and similar cases has been widely used for the detection of regional stress and deformation fields (e.g., Scheidegger, 1980, 2001; Andeweg, 2002; Decker et al., 1993; Ghisetti, 2000; Lopes Cardozo and Behrmann, 2006; Oncken, 1988; Pischinger et al., 2008). It consists simply in bisecting the obtuse angular distance between the poles of the "true" conjugate planes in the stereo-net for finding the σ_1 axis; σ_3 bisects the acute angle and σ_2 corresponds to the pole of the great circle connecting the poles of conjugate fractures (Fig. 3 b).

3.2 Faulting-related secondary fractures

This association (Fig. 3 c, Fig. 5, Fig. 6) mainly combines shear planes with systematic geometrical arrangement preceding and accompanying the formation of through-going fault structures (Riedel, 1929; Anderson, 1951; Skempton, 1966; Moore et al., 1989; Logan et al., 1979, all based widely on the Coulomb idea of internal friction, the φ angle concept). In nature, however, rarely all these potential shear planes are verified and existing, e.g., both R_1 and R_2 (mechanically equivalent features) are rarely equally developed, because their individual formation depends much on the relative magnitude of effective stresses acting parallel (σ//´) and perpendicular (σ⊥´, symbols after Mandl, 2005) to the evolving brittle shear

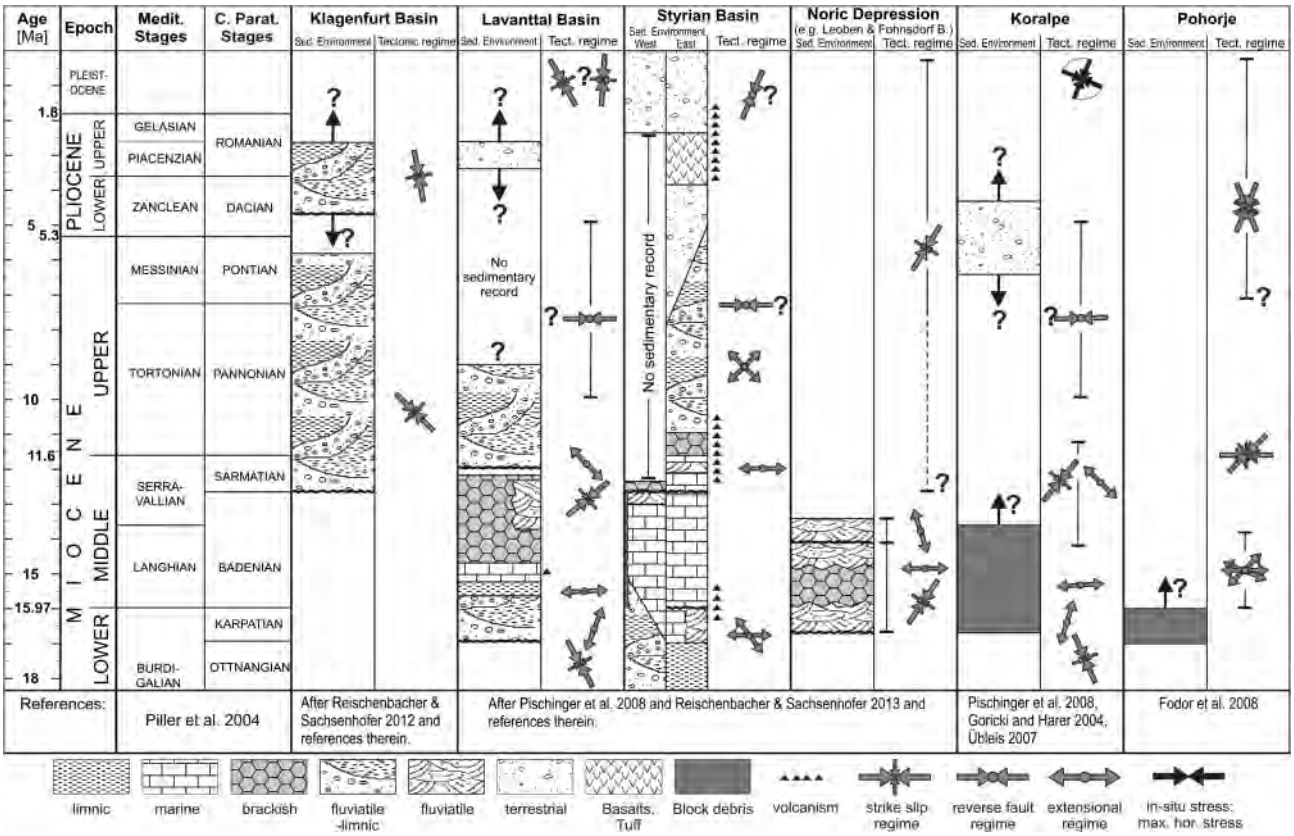

Figure 2: Schematic correlation of the sedimentary evolution and the paleostress regime for the Klagenfurt, the Lavanttal and the Styrian Basin, as well as for the Noric Depression, the Koralpe and the Pohorje from the Ottnangian (Lower Miocene) to Pleistocene.

zone (Fig. 5). In the initial stage of shear zone development a shear zone boundary (SZB) or a Y-shear have not yet been localized (Fig. 7 a). In this stage a high σ//´ favours the development of the antithetic R_2 (and P?) structures (Fig. 7 b), while a comparatively low σ//´ fosters the generation of R_1 (and X?) shears (Fig. 7 c; Mandl, 2005).

In the field the presence of a clear SZB or Y-shear was a prerequisite, to assign the mapped fractures to this structure group (Fig. 6). Isolated fractures were assigned to the conjugate shear fracture group (see chapter 3.1).

For the purposes of graphical analysis (Fig. 3 d) the direction of the maximum compressive stress σ_1 bisects the acute angle ([90-φ]°) between synthetic R_1 and antithetic R_2 Riedel shears. They ideally make angles of (φ/2)° and (90-φ/2)°, respectively, with the Y-shear or the SZB. The orientation of σ_2, theoretically coinciding with the pole to the $\sigma_1 - \sigma_3$ great circle, is given by the intersection of shears with the SZB or the Y-shear. In this study Y and R_1 shears were used for construction of stress axes.

Shears labelled P and X in Fig. 5 may be explained as results of the continuing fracture generating mechanisms and kinematic processes (Mandl, 1988, 2000). They are of low value for a reliable graphical determination of “paleostress” axes, because their generation and angular relationship are not well established.

The Y-shear, once formed by the coalescence of various precursor shears, marks the plane of theoretical maximum exposed shear stress parallel to the SZB. At least initially, σ_1 is inclined at an angle of θ = 45° to it. Note that all these considerations do not apply, e.g., to polymodal fault patterns that may form within a single stress field, where at least some faults cannot contain the intermediate principle axis (Krantz, 1988; Reches, 1978; Reches and Dietrich,

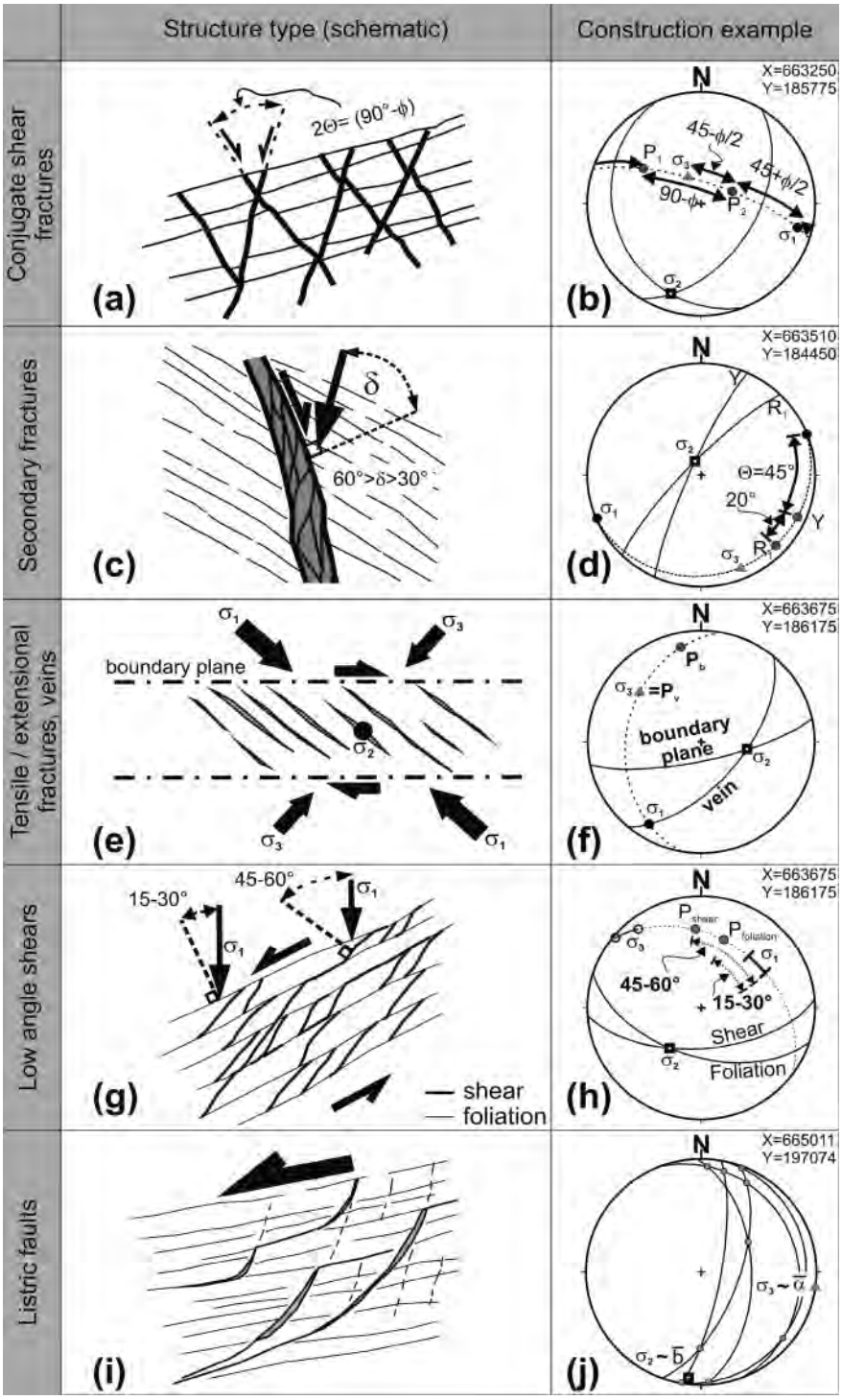

Figure 3: Analysed structure types and the respective construction of paleostress axes. (a) Conjugate set of shear fractures with σ_1 bisecting the acute angle between the two shear fractures. (b) Construction example for the determination of the paleostress orientations for a given set of conjugate shear fractures (reverse sense of shear, lower hemisphere). (c) Shear zone and related fractures (sinistral sense of shear, see Fig. 5 for nomenclature of fractures). (d) Construction example for the determination of the paleostress orientations for a Y-shear and an associated Riedel shear (strike slip kinematics, dextral sense of shear, lower hemisphere, abbreviations refer to Fig. 5). (e) Vein development and the theoretical orientation of the principal stresses. (f) Construction example for the determination of the paleostress orientations for a given set of veins and the respective boundary plane (lower hemisphere). P_v labels the pole to the vein, P_b the pole to the boundary plane. (g) Low angle shears, bold lines indicate the shear planes, thin lines the metamorphic foliation. (h) Construction example for the determination of the paleostress orientations for low angle shears (lower hemisphere). Only ranges can be given for σ_1 and σ_3. P labels the pole to the respective great circle. (i) Listric normal faults. (j) Construction example for the estimation of the azimuth of σ_2 and σ_3 from listric planes, σ_1 is assumed to be vertical. $\bar{b}$ and $\bar{\alpha}$ denote the mean intersection axis and the mean azimuth of the measured planes.

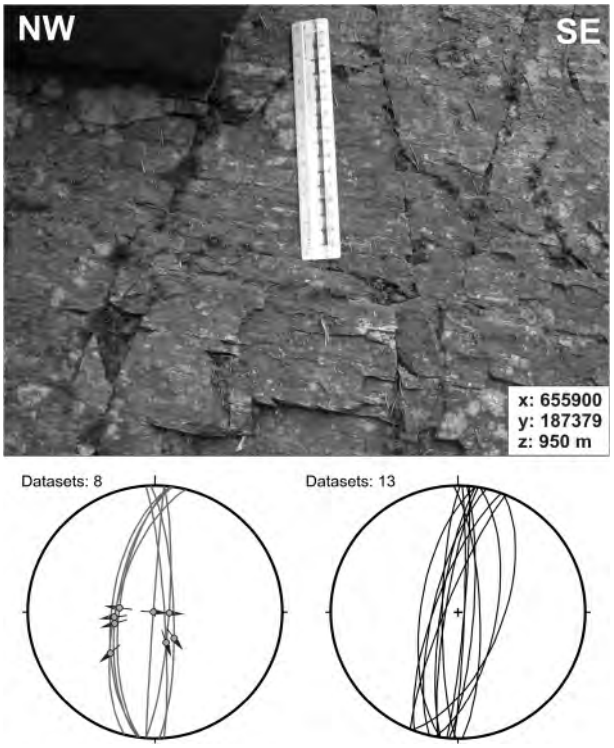

Figure 4: Outcrop in "Plattengneis" mylonite, exposing conjugate shear planes with (Angelier plot, left side) and without striation (right plot). Conjugate shears with striations constrain W-E directed extension of shears without striation. Note eastward displacement along foliation parallel shear plane below the scale bar. Equal-area projection, lower hemisphere. Scale in photograph is 15 cm.

1983; Reches and Lockner,1994).

3.3 Tensile/extensional fractures, veins

These features (Mandl, 2000) are generally thought to be generated either under uniaxial tension as tensile fractures with $\sigma_3' = -T_0$ and $\sigma_c' =\sim 0$, with $\sigma_c' = \sigma_1' < 3*|T0|$) or otherwise as extension fractures ("cleavage fractures") under uniaxial compression with $C_0 = \sigma_1' \geq 0$ and $\sigma_3' = \sigma_c' = 0$; possibly due to elevated pore fluid pressure (σ_3', σ_1': minimum and maximum effective normal stresses; σ_c': confining pressure; T_0: tensile strength of the material; C_0: uniaxial compressive strength).

From simple calculations it is well known that tensile fracturing, as being dependent on pore fluid pressure and tensile material strength (with few exceptions) is restricted to the uppermost kilometres of the lithosphere. However, even veins need not necessarily to originate as tension or extension fractures, since shear fractures in brittle rocks may open up in a dilational bookshelf-type rotation (see Mandl, 2005). In the ideal case, tensional/extensional open fractures or filled dykes and veins may have opened perpendicular to the local axis of the least principal stress σ3 (Fig. 3 e) and hence contain the σ_1 and σ_2 axes within their plane (e.g. Bons et al, 2012). Consequently, the σ3 axis is directly represented by the poles to the fractures in the projection net (Fig. 3 f), the other principal stresses lie within the plane of the fracture and no reliable localisation is possible without additional information.

These en-echelon fractures sometimes array in conjugate brittle shear bands. Small-scale extensional fractures branching off from master features provide the required additional information (see above) by the intersection linear between the latter fractures and the master feature or a (real or virtual) boundary plane, respectively. Such supplementary features could be e.g. feather fractures, pinnate joints, "wing" cracks and "dogleg" fractures, "pennant veins, flag veins" (Coelho et al., 2006).

This real or virtual intersection may be taken as marking the intermediate principal stress σ_2 (see discussion below). Accordingly, the direction of σ_1 can be found 90° off σ_2 on the great circle representing the planes of the tensile/extensional fractures. The locus of σ_3 coincides with the poles of the latter (Fig. 3 f).

3.4 Low-angle-shears

This term refers to the generally low acute angle (10° < β < 40°) between certain brittle shear planes and foliation, the main element of anisotropy (Fig. 3 g, Fig. 8). Slip on foliation (and other rock mass discontinuities) results in a pattern of very acute-angled, small rhombohedral discontinuity-bound rock elements. These structures may resemble flat-and-ramp geometries at a cm- to m-scale. In cases, these shear planes show slight polishing and a faint striation (Fig. 8). Displacement markers indicate normal to strike-slip sense of shear accompanied by a certain slip along foliation planes.

Considerations on generating stresses are difficult and studded with pitfalls as foliation anisotropy plays a major role both in local stress distri-

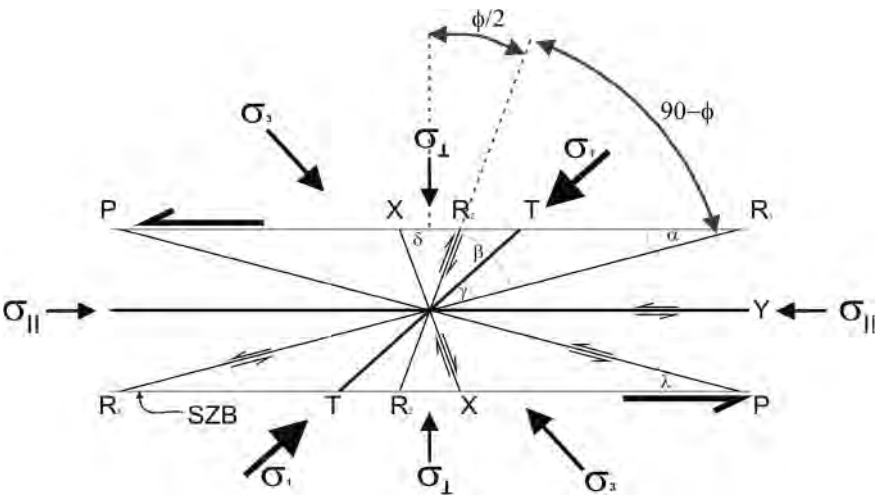

Figure 5: Fracture associations in a shear zone (after Logan et al. 1979). Stress nomenclature follows Mandl (2000).

bution and displacement kinematics (Donath, 1961; Marrett and Allmendinger, 1990; Price and Cosgrove, 1990; Peacock and Sanderson, 1992). The presented analysis assumes that the axes of σ_1 and σ_3 are contained in a normal plane to both shear fractures and foliation and that the angle of σ_1 to the foliation is $90 > \theta >> 45°$. For the construction an angular range of 15° to 30° (i. e. $75° > \theta > 60°$) between the pole of foliation and the assumed orientation of σ1 has been adopted (Fig. 3 h, and Gomez-Rivas and Griera, 2012, Fig. 1). Accordingly, only ranges of potential directions of stress axes are given in Figure 3 h.

It is inferred that in nature these geometric constraints are appropriate to prevent the foliation planes from slippage, thereby promoting the development of prominent new low-angle shear fractures. In cases, low angle shears are linked to listric fractures, indicating precursor structures to listric faults.

3.5 Listric faults

Listric planes are prominent elements in gravity-driven extensional tectonics and there is ample literature, in particular on large-scale structures in soft sediments with respect to basin development (e.g., Patalakha, 1986; Ramsay and Huber, 1987; Bradshaw and Zoback, 1988; Dula, 1991; Ellis and McClay, 2007). Both, σ1 and σ3 would have to form a non-uniform field within a given plane of observation (constant orientation of σ2), so as to allow the generation of listric faults. Their potential generation as smooth, coherent fault surfaces in brittle tectonics and in agreement with Coulomb fracture principles has been presented and proven by Mandl (1987, 2000).

However, the use of listric structures in kinematic studies within brittle rock is not well documented. In the Koralm, at several sites well developed listric planes of the cm- to 10 m-scale, sometimes in a cross-sectional staircase-geometry, can be found (Fig. 9, Pischinger et al., 2008). The exposed flats are generally (sub-) parallel to the planes of foliation and the sense of displacement is normal (Fig. 3 i). They have not been observed in areas with a pronounced dip of foliation. It is not intended here to discuss the nature of the curved planes in terms of responsible stresses for their generation. Based on fault slip data (Fig. 9) and shear sense indicators we adopted the working hypothesis that the very small displacements observed in our examples might indeed have happened almost perpendicular to the axis of curvature. Constructed b-axes of the curved part of surfaces are considered as being at right angles to the incipient displacement along the structure within the foliation planes (Fig. 3 j). The azimuth of σ3 can be assu-

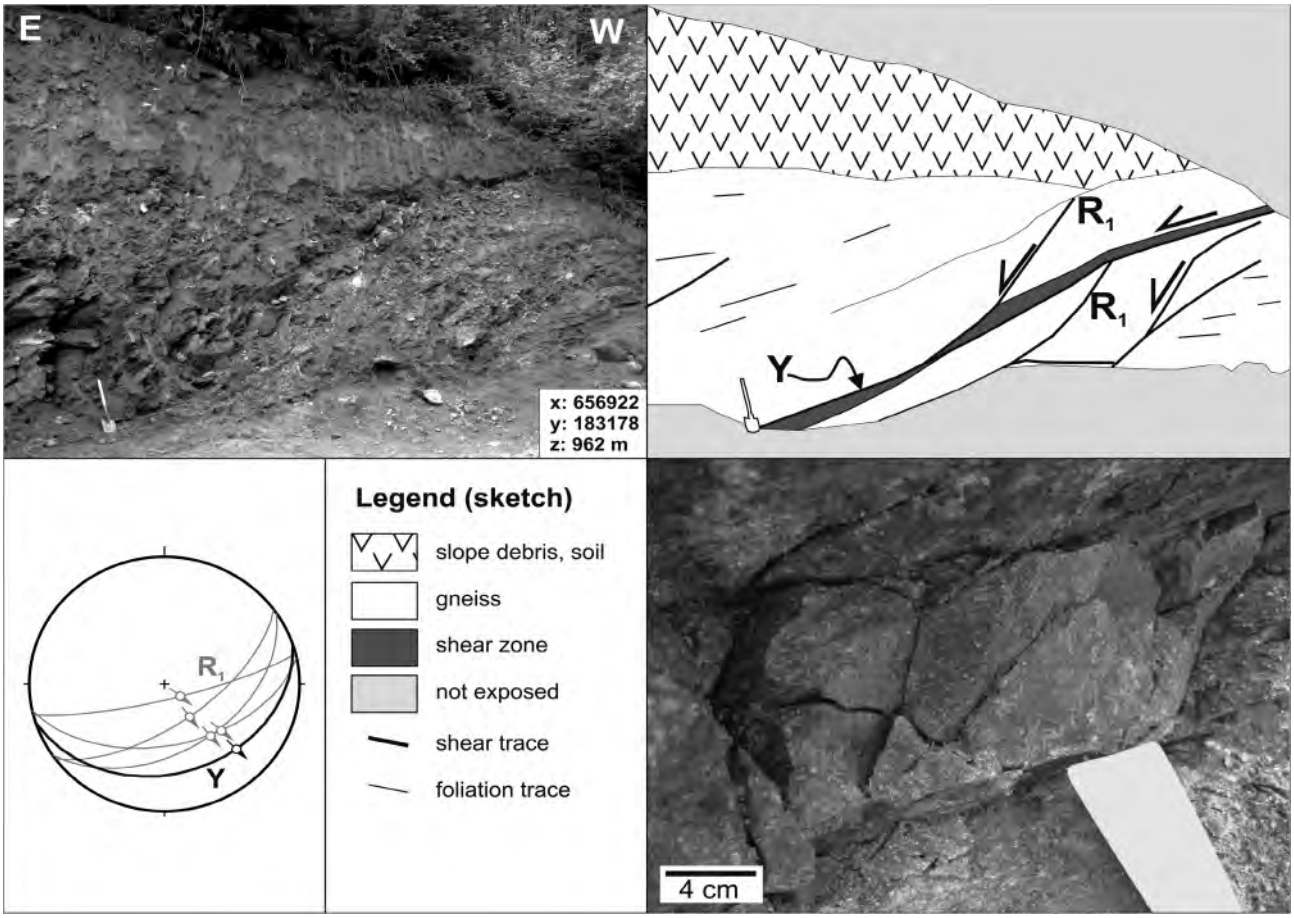

Figure 6: Faulting related secondary fractures of a cataclastic shear zone with normal sense of shear in gneissic bedrock of the eastern Koralpe. Y-shear - Riedel shear configuration is observable on the outcrop (spade is approx. 60 cm long) and the hand specimen scale (lower right, picture was taken just left of the upper left photograph). Angelier plot (Equal-area projection, lower hemisphere) shows orientation and sense of shear for the Y-shear (black great circle) and several Riedel shears.

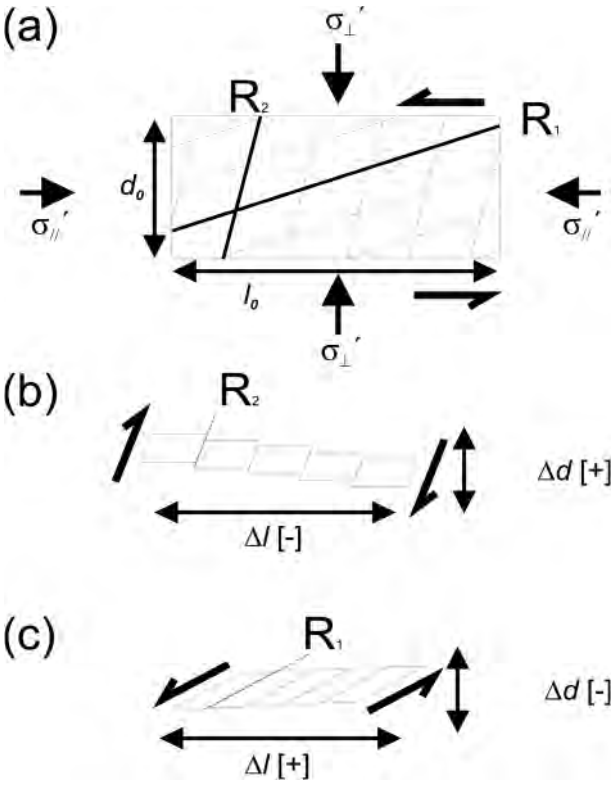

Figure 7: Initial shear zone development, where the formation of R_1 and R_2 is equally probable: (a) Geometry for the development of initial shear planes, (b) comparatively high σ//´ leading to preferred development of R_2, (c) comparatively low σ//´ causing the development of R_1. SZB; Y- and P- shear elements have not yet developed for the depicted stages (l_0…initial length, d_0… initial thickness).

med to be equivalent to the mean dip direction of the measured segments of the listric fault plane.

4. Results

4.1 Structures

4.1.1 Conjugate shear fractures

According to the graphical analysis of our field data (Tab. 1 in Online Appendix) all three main "Andersonian" fault types are present. However, the constructed stress axes for the most part are considerably inclined (Fig. 10 a, b, c; Tab. 2 in Online Appendix).

Fractures associated to "normal" faulting are characterized by a subvertical σ_1 and slightly inclined σ_3. The latter show two preferred, partly overlapping directions of extension (WNW-ESE/E and SW-NE), while the σ_2 axes scatter around northern and southern plunge directions (Fig. 10 a).

Structures with a sub-vertical σ_2 (strike-slip) show a considerable scatter in the orientations of the slightly plunging to horizontal σ_1 stress axes. Two subsets are indicated, one with SSW-NNE, and one with NW-SE orientation. The constructed σ_3 axes are concentrating subhorizontally in WNW-ESE and in SW-NE to NNE direction (Fig. 10 b).

The associations exhibiting reverse kinematics are characterized by σ_3 axes plunging steeply to northern and southern directions, while σ_1 plunges flatly around the E-W axis (Fig. 10 c). The axes of σ_2 dip moderately steep to towards SSW and NNE.

4.1.2 Faulting-related secondary fractures

The stress axes directions constructed from these structural elements (for the most part Riedel shears, Tab. 1 in Online Appendix) also may be attributed to the three main Andersonian faulting types:

Normal shears display scattering, steeply plunging axes of σ_1 (preferably to the W to N sector) and a remarkable concentration of σ_2 axes plunging flat to moderately steep to SE-SSW. Consequently, the flat σ_3 axes scatter around E-NE directions and may be subdivided into two clusters (Fig. 10 d). A single datum indicates extension in NW-SE direction.

Structural associations with strike- slip character show steep σ_2 axes and a noticeable regularity in the orientation distribution of the remaining two stress axes. Both dextral and sinistral senses of displacement are constrained by the field data. The sub-horizontal plunging σ_3 as well as σ_1 axes trend NNW-SSE and WSW-ENE (Fig. 10 e). Subordinate, flat to moderately steep plunging σ_1 axes cluster in the NW.

Structures with reconstructed steep to subvertical σ_3 axes are interpreted as reverse shears. Despite the pronounced scatter, certain aggregations may be seen for the horizontal axes of σ_1 trending WNW - ESE and SW - NE respectively (Fig. 10 f). The axes of σ_2 scatter considerably too, yet roughly three clusters can be distinguished (NW-SE, SSW-NNE and N trending). The σ_3 orientations are generally steeply inclined (>56°), and concentrate around NNE and SE-SW plunging axes.

4.1.3 Tensional/extensional fractures, veins

The synoptic diagram (Fig. 10 g) depicts the poles to the tensional/extensional fractures and veins (Tab. 1 in Online Appendix) as they are supposed to represent the orientation of σ_3 axes - at least on a local scale. The very steeply dipping to sub-vertical structures yield two pronounced clusters of σ_3 axes: NNW to NNE, and W-E to WNW-ESE. Two data trend towards SSW. The first group consists almost exclusively of open gashes, while in the latter open and mineralized veins (chlorite plus quartz, calcite, feldspar, etc.)- are present in quite equal amounts (Fig. 10 g).

4.1.4 Low angle shears

These structures are difficult to analyse in terms of Mohr-Coulomb failure conditions because of the pronounced rock anisotropy and the uncertainty concerning the mechanical role of schistosity.

In the cumulative diagram (Fig. 10 h) the constructed ranges of potential σ_1 directions with a few exceptions seem to be arranged (with steep to subvertical plunges) along two girdles: a steeply N-dipping E-W- great circle and a broader girdle along approximately N-S striking very steeply W-dipping great circles. Consequently the axes of σ_2/ σ_3 are arranged in a broad band

along the periphery of the cumulative diagram (σ_2 axes a).

A closer look to the preferred stress axes orientations (Tab. 3) allows to distinguish tentatively five groups:

Group 1 stress axes orientations were derived from several outcrops. They display steeply to very steeply plunging σ_1 axes towards NW-N and consequently flat to sub-horizontal σ_3 in NW-SE direction. The axes of σ_2 plunge moderately steep to flat towards S and SE respectively.

Group 2 is characterised by moderately steep to sub-horizontal σ_2 axes plunging to SE and very flat SW-SE orientations of σ_3.

Group 3 comprises assemblages with distinctly E plunging σ_2 axes and consequently flat to subhorizontal σ_3 in N-S directions as well as a steep W dipping σ_1.

Group 4 displays steeply to very steeply plunging σ_1 axes towards SW, consequently flat to sub-horizontal σ_3 in NW–SE direction. The axes of σ_2 plunge moderately steep to flat into the NE sector.

Group 5 data, come from two outcrop series only. Axes of σ_2 are concentrated in N to NW directions with a flat plunge and hence σ_3 axes cluster in flat W to SW directions. Constructed moderately to very steep σ_1 axes directions dip steeply towards ENE–SSW.

Groups 2 and 5, as well as groups 1 and 4 are different just in the opposite dip directions of the constructed ranges of σ_1 and σ_2 axes, so they may be attributed to the same stress regime.

In their vast majority the low angle shears seem to be related to three normal faulting stages with extension in NW-SE to WNW-ESE, SW-NE and N-S directions. Strike-slip faulting is only reflected by a few single values.

4.1.5 Listric faults

In the cumulative diagram (Fig. 10 i) correlating poles of measured listric planes are connected by broken lines. Almost all trails point to the midpoint of the diagram, so the related constructed b-axes plunge flatly to (sub-)horizontally. They cluster along the W to SW and E to NE, as well as along the NNW-SSE directions. Those “b-axes” are considered to represent the σ_2 orientation. Generally the data confirm extension mainly in NNW-SSE to WNW-ESE as well as in SW-NE direction. The σ_2 pattern shows similarity to the one established for the low-angle shears.

4.1.6 Fault-slip data from the Styrian Basin

New constraints on the timing of faulting have been gained during excavation of tunnels within Badenian sediments (Florianer beds) of the Styrian Basin in vicinity to the Koralpe. Here, a fault bounded horst structure was excavated. Fault slip data document extension mainly in WSW-ENE to SW-NE

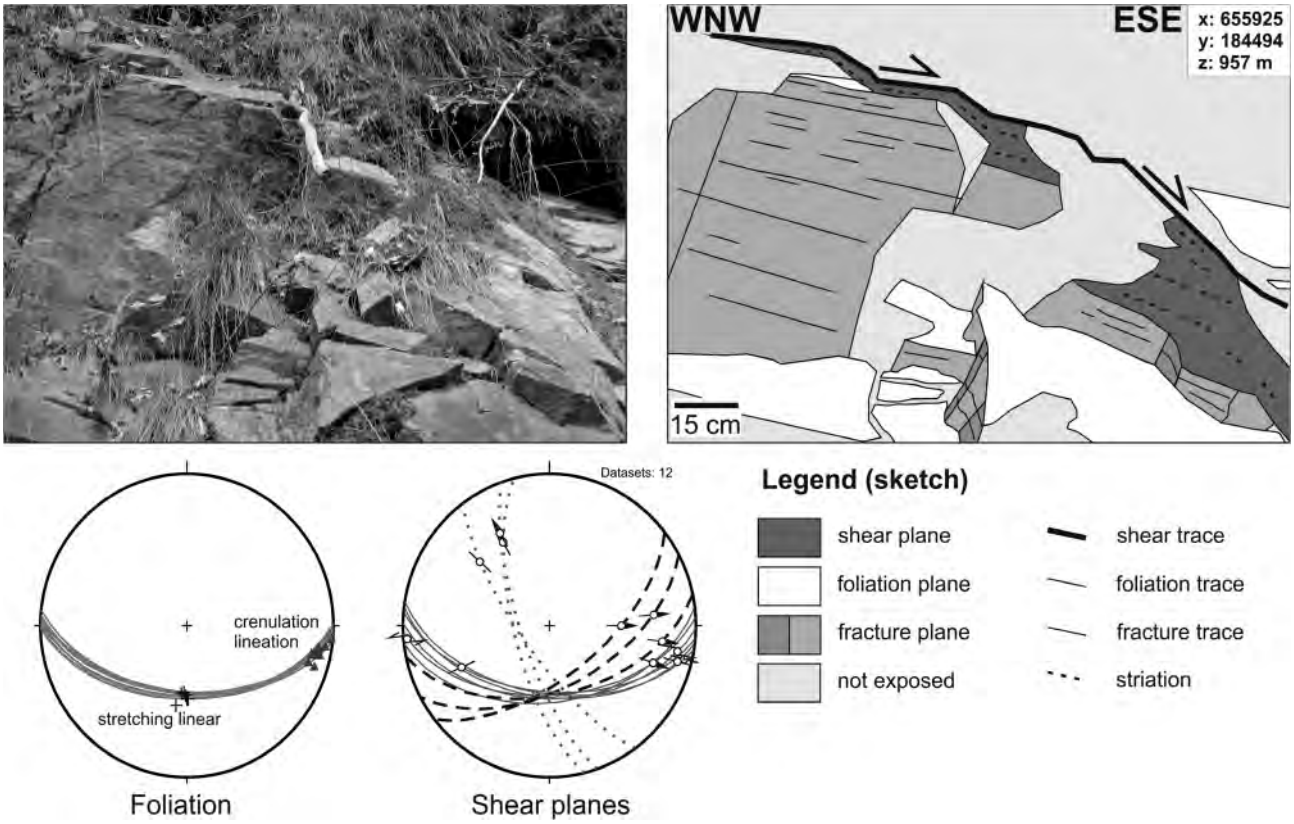

Figure 8: Outcrop in "Plattengneis" mylonite of the central Koralpe, exposing low angle shear planes and shearing of foliation. Left Equal-area projection (lower hemisphere) displays foliation with stretching (crosses) and crenulation lineation (triangles). Right diagram (Angelier plot) shows low angle shears (dashed great circles), slightly steeper than foliation parallel shears (continuous great circles). Steep WSW dipping shear planes (dotted lines) are not visible in the photograph. In this location striations indicate strike-slip displacement. Striations plot in similar direction as crenulation lineation, but are clearly distinguishable from the crenulation lineation.

direction (Fig. 11 a, b & d). These directions may correlate with the D2 event (Pischinger et al., 2008) and would not contradict ist early Badenian timing. Further fault slip data indicate a second event of extension in NNE-SSW direction (Fig. 11 c). This direction of extension would correlate with the D1-2 event, which was assigned to the Karpatian. As the age of the faulted sediments is generally agreed to be Badenian, this would imply that this faulting must be younger than or at least Badenian in age. However, no age relationships could be documented for the faults from the Styrian Basin.

4.2 Regional Analysis

For a regional comparison of the derived paleostress orientations, the data of the individual structures were grouped according to the three basic Andersonian fault types. The vein data were treated as a separate group, as they could be related to all three types of faulting. Further, mean paleostress axes were calculated for the individual outcrops, if several estimates with similar paleostress orientations existed within an outcrop. This reduces the effects of local scatter and allows a better comparison of the data in the map. Estimates derived from different structure types were not merged during this averaging process.

Generally, the analysed structures were mapped in three regions of the Koralpe (refer to Fig. 1 and Fig. 12 d for locations): The first is located within the western slopes of the Koralpe towards the Lavanttal Basin, in the vicinity to the Lavanttal fault system. The second is situated in the central eastern Koralpe, approximately 6 to 10 km SW of Deutschlandsberg. The third one is within 2 km from the eastern mountain front of the Koralpe towards the Styrian Basin. The horizontal distance between the easternmost and the westernmost outcrops is more than 20 km.

The data attributable to normal faulting are dominated by σ_3 axes scattering between SW-NE and NW-SE (Fig. 12). In the W (Fig. 12a) the σ_3 axes trend predominately WSW-ENE, roughly perpendicular to the general strike direction of the regional faults, indicating normal fault kinematics for these faults. Additionally a few data indicate extension in NNW-SSE to NW-SE direction. Compared to the west the outcrops in the central eastern Koralpe (Fig. 12b) show a pronounced scatter in their σ_3 orientation, although the trend visible in the data from the West is still recognisable.. At the eastern margin of the Koralpe the σ_3 data indicate clearly extension in W-E direction (Fig. 12c).

Following the data with strike slip kinematics (mainly conjugate fractures and fault related minor shears, Fig. 10) two clusters of stress orientations can be distinguished within the entire data set: The first is characterised by NW-SE to NNE-SSE directed compression and extension in WNW-ESE to SW-NE direction. The second constrains compression in approx. WSW-ENE and extension in NNW-SSE direction. In the stress axis map the latter is more prominent in the easternmost Koralpe, whereas the central and western outcrops are dominated by the first cluster (Fig. 13).

Reverse kinematics was mapped in all three working areas (Fig. 14). The directions of compression range from WNW-ESE to WSW-ENE. Map analysis shows that σ_1 orientations resemble the σ_1 orientations of strike slip related structures, mainly found in the east of the working area. A formation of these features within compressional domains of the strike slip faults could be used as a possible explanation for their genesis.

As described above, for the vein data only the smallest principal stress direction σ_3 is obtained. Two sets indicate prominent WNW-ESE to WSW-ENE extension and less frequent NNW-SSE to NNE-SSW extension respectively (Fig. 15). The estimated smallest principal stress directions (σ3) coincide largely with the normal faulting data (Fig. 12), and it seems tempting to assign both to the same tectonic stages.

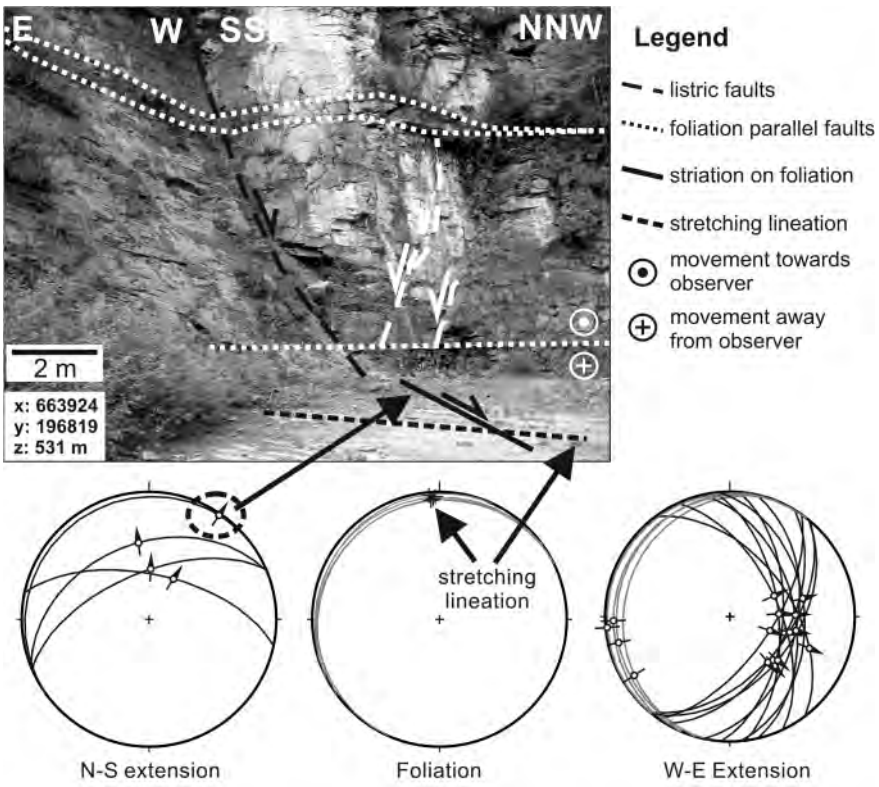

Figure 9: Quarry in Plattengneis (NW of Stainz, Eastern Koralpe): Southern wall of quarry follows a north dipping listric normal fault which ends in a foliation parallel shear plane. Striation on foliation parallel shear is different from metamorphic stretching lineation. Eastward dipping listric shears, which end in a foliation parallel detachment zone, indicate W-E directed extension in the east facing quarry. Cross cutting relationships indicate that W-E extension is younger than N-S extension.

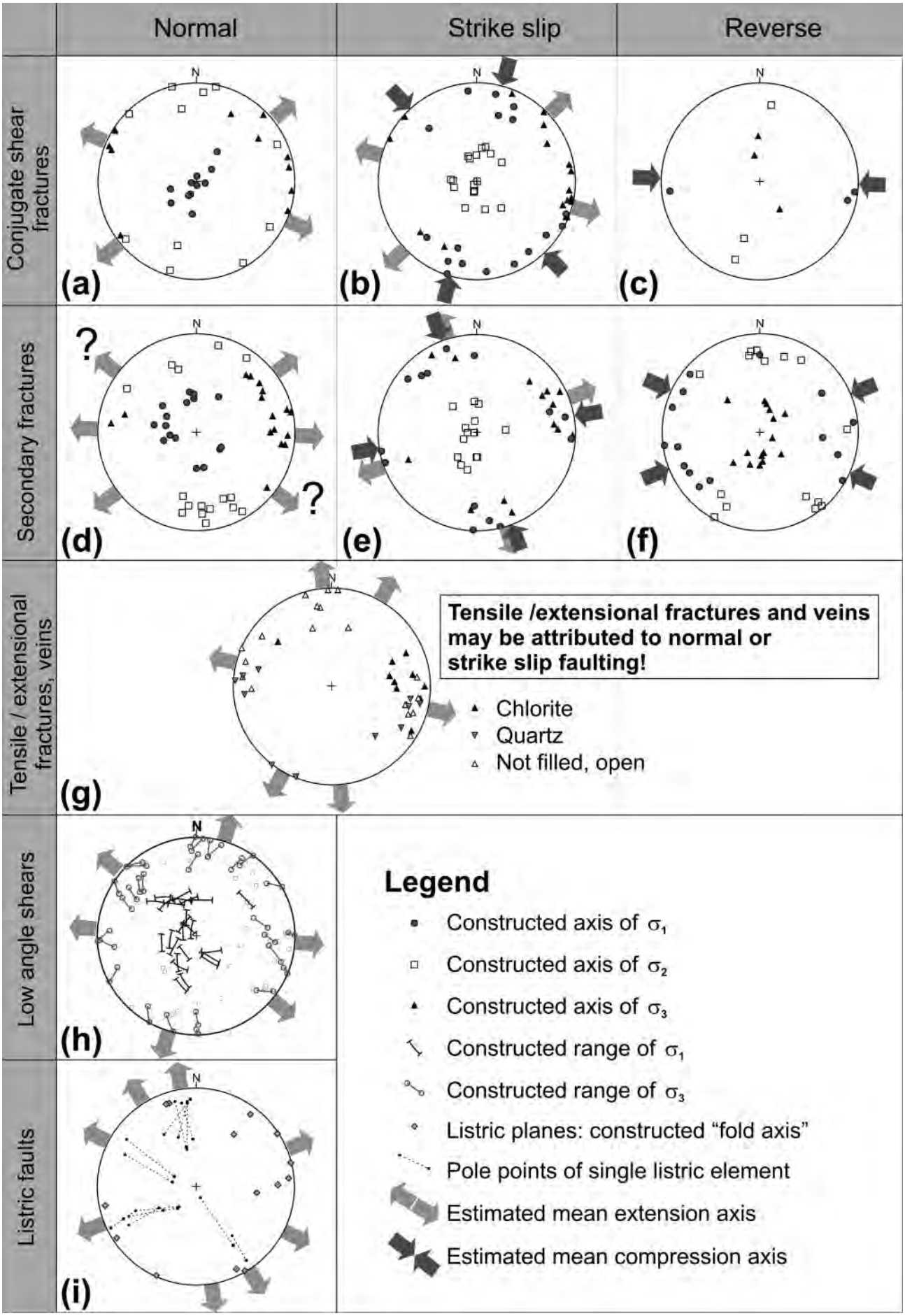
Normal
Strike slip
Reverse
Conjugate shear fractures
Secondary fractures
Tensile / extensional fractures, veins
Low angle shears
Listric faults
N
(a)
(b)
(c)
?
?
(d)
(e)
(f)
(g)
(h)
(i)
Tensile /extensional fractures and veins may be attributed to normal or strike slip faulting!
Chlorite
Quartz
Not filled, open
Legend
Constructed axis of σ1
Constructed axis of σ2
Constructed axis of σ3
Constructed range of σ1
Constructed range of σ3
Listric planes: constructed “fold axis”
Pole points of single listric element
Estimated mean extension axis
Estimated mean compression axis

5. Discussion

5.1 General considerations

The methodology described in this paper is not particularly novel, however, not widely known and rarely applied. The latter may be caused by the difficult identification of some of the structural associations and the frequent ambiguity in their interpretation.

However, if one accepts the well-founded concept that brittle fracture associations do reflect their generating stress conditions in a reproducible way, it should be justified to use them for a tentative determination of paleo-stress axes orientations, or at least for the identification of instantaneous stretching/shortening axes. This is actually done based on evaluated strain/displacement directions documented in the field. Evidently enough, not all features have the same explanatory power, and some can only be used with utmost caution and only in combination with more robust methods.

To avoid a biased data pool by an unequal number of measurements, the calculation of paleostress mean vectors for the individual outcrops and structures is essential. Calculation of mean vectors (Wallbrecher, 1986) is nowadays a standard routine, implemented in a number of software packages (e.g. Reiter and Acs, 1996-2007).

The application of traditional hemispherical projection techniques bears no problems as long as directions and angular relationships (geometry) are under consideration. Effects of rock anisotropy, however, cannot be considered satisfactory (nor at present by other widely used paleostress detection/interpretation methods!), without major assumptions. Resolved shearing stresses on planes inclined to the principal stress directions depend both on the absolute and relative magnitudes of principal stresses (namely the stress ratio) and are generally not related in a simple way to the principal stress directions (Bott, 1959; Jaeger, 1959, 1960; Jaeger and Cook, 1979; Goodman, 1976; Treagus, 1986; Lisle, 1989; Priest, 1993; Blenkinsop, 2008). Furthermore, the degree of anisotropy, i.e. the difference in the magnitude of Coulomb-Navier strength parameters between the “intact” material and the planes of weakness plays a major role, and still little information about the latter exists for the rocks under consideration (Brosch et al., 2000). Consequently, homogeneous, isotropic material with Coulomb-type (“Andersonian”) fracturing/faulting behaviour as well as a symmetrical stress tensor with homogeneous stress field are most likely to be implicitly assumed in structural geological models for the inverse analysis of initiation and kinematics of faulting, and the related stress configuration. Another major drawback is the tacit implication that fault planes do contain, and intersections of shears with associated extension fractures do define the axis of σ_2. For polymodal fault sets and faults developing from most favourable planes of interaction of mode-I cracks, or re-activated shear zones, this altogether does not necessarily apply (Healy et al., 2006).

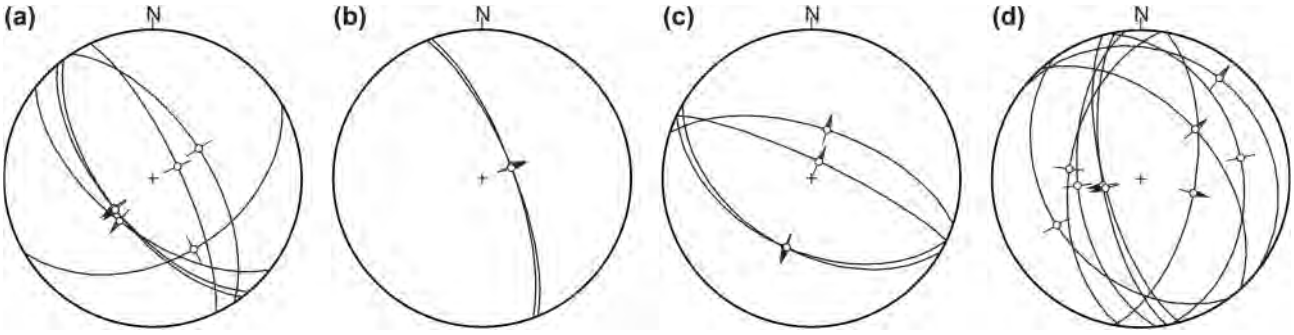

Figure 11: Fault slip data of faults within Badenian sediments (Location: KAT1 tunnel, approx. 5 km east of Deutschlandsberg). Angelier diagrams were drawn with the Tectonics FP program (Reiter and Acs, 1996-2007). For explanation see text.

As for conjugate shear fractures it is important to note that not any configuration of discontinuities making acute interplane angles (β) of approximately $45° < \beta < 75°$ may be termed “conjugate”: common and practically synchronous origin as mode-II fractures, as well as compatible initial displacement patterns are required. The necessary evidence for conjugate origin is usually obtained from structures with unique kinematic significance (e.g. faults) nearby the fractures. A major difficulty in practice lies in the identification of shear-related origin and displacement mode of “true” conjugate fractures, because of the mutual kinematical arrest of both mechanically equivalent elements. Only one shearing element is free for displacement at a certain instant, the other gets blocked and remains inactive, if not the “double gliding” mechanism is active (Mandl, 2000). Furthermore, due to the influence of superordinate structures, the local principal stress orientations may significantly deviate from the regional trend (Engelder and Geiser, 1980, Rawnsley et al., 1992, Petit et al., 2000).

All this may warn against indiscriminate use of discontinuity patterns for the reconstruction of far-field paleostress orientations. However, the same holds true for, e.g., fault slip data analysis, which in the same way may render results only characteristic for the interior of a broader belt of deformation and

Figure 10: Constructed paleostress axes and estimated kinematic axes for the analysed structures.

representative for the “true” regional geometry of paleostress. This fact would be worth a discussion of scale dependence of observation. It is not before a regional synopsis of stress orientation data and fault pattern that a plausible interpretation with respect to far field stresses is possible.

The actual nature of the reported low-angle shears is difficult to explain and the mechanics leading to their formation may be quite complex. In particular, the role of strong rock anisotropy cannot be appropriately considered, since reliable respective mechanical data are not at hands. Therefore a quite large angular range for the potential orientation of stress axes has been selected, based on the relevant literature. Finally, the angles between planes of weakness and a newly forming fracture in an anisotropic medium may change, depending on stress magnitudes and stress ratios (e.g. Jaeger, 1960). According to Barron (1971), in an anisotropic material the primary (initial) crack is not necessarily oriented critically – as it is the case in isotropic media. Furthermore, secondary planes of weakness (away from the visible foliation) have to be considered as has been shown in microfabics studies (e.g. Brosch et al. 2000: microcrack concentrations parallel to the XY-plane of the fabric) and in numerical and analogue tests (e.g. Tang and Hudson, 2010).

For the structural analysis of veins there is a high risk of misinterpretation of initiating shear couples, if virtual boundary planes are constructed erroneously along the ends of the ex-

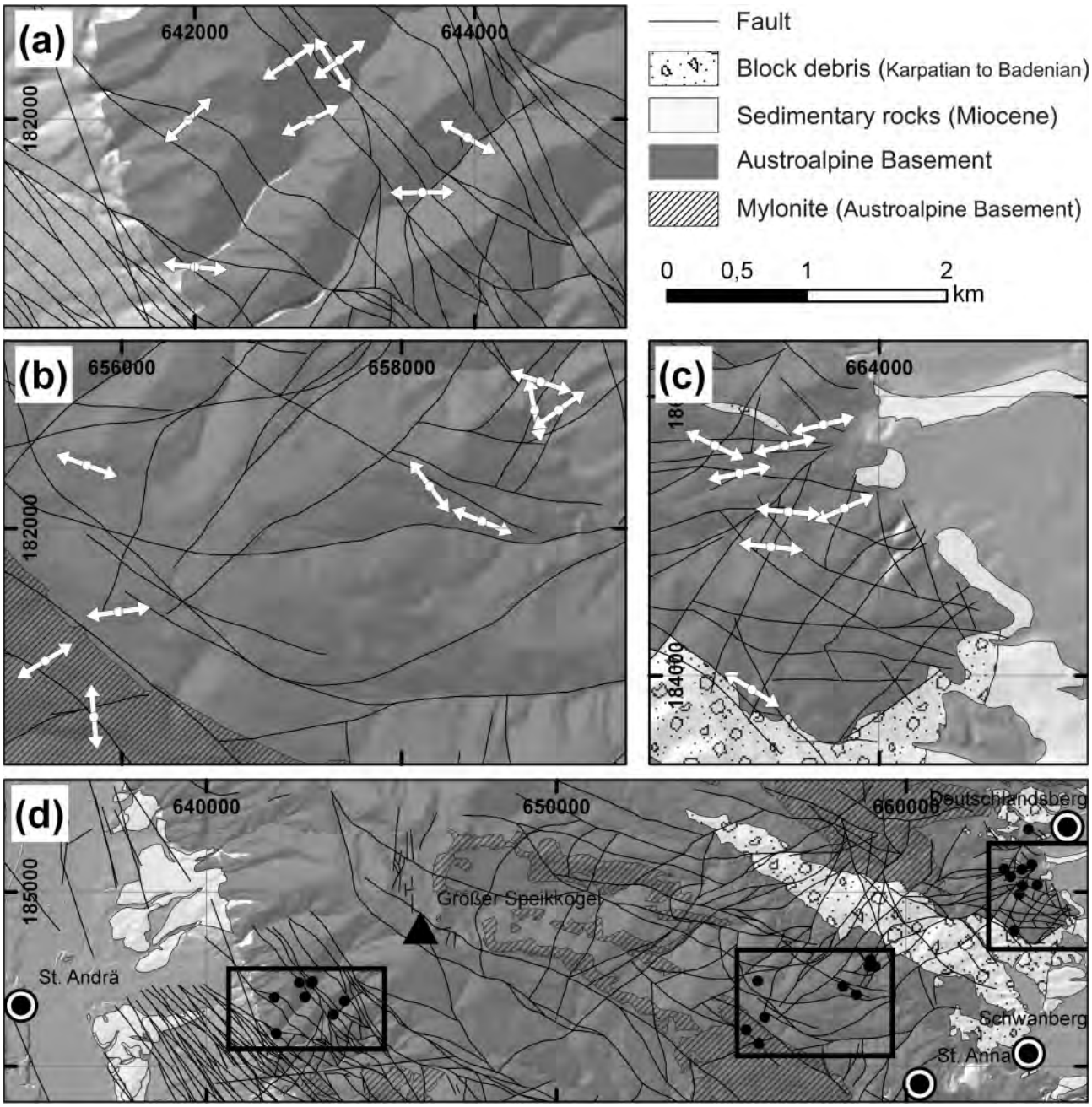

Figure 12: Regional distribution of the paleostress axes with normal fault kinematics. Grid is in Austrian BMN M34 system. 10 m resolution DEM provided by Bundesamt für Eich- und Vermessungswesen (Vienna).

posed vein traces. Therefore, limited exposure of the analysed vein traces and the actual vein orientation have to be considered (Fig. 16). For the ranges of potential inclinations of pre-peak brittle shear zones to the external σ_1' direction, see Mandl (2005).

In conjugate shear zones consisting of en-echelon veins or open gashes the bisector of the acute inter-limb angle may be taken as the σ_1 compressive axis and the orientation of the intersection linear of the zones as the direction of σ_2. If the individual branches of conjugate bands show a mutually non-parallel orientation of the individual veins or gashes, the analysis only renders the principal directions of a very proximate local and perturbed stress field. The analysis gets unreliable if the fractures/veins exhibit sigmoidal distortion or the dilational bookshelf-rotation is to be suspected as the opening mechanism. Anyway, it may be very difficult to measure reliable orientations of en echelon fractures/veins and of the related shear-zone boundary planes, because they usually appear as linear traces in the outcrops and not as planar structures.

Veins arranged en echelon or bands of brittle fractures may be produced "...by more than one mechanism" (Olson and Pollard, 1991) and, considering the range of orientations that en echelon shear and tension fractures may share, it is often difficult to decide upon the primary generating mode (tension/extension-, hybrid-, shearing-modes), or secondary activation mechanisms.

Considering the analysis of listric planes the axis of curvature on geometrical reasons may not be oriented perpendicular to comparatively large displacements along a listric surface. The more so, as the detailed analysis of listric planes frequently exhibits their non-cylindricity or multi-cylindricity, respectively.

Based on striations on the slip planes we adopted the working hypothesis that the very small displacements observed in but a few examples might indeed have happened almost perpendicular to the axis of curvature (Fig. 9).

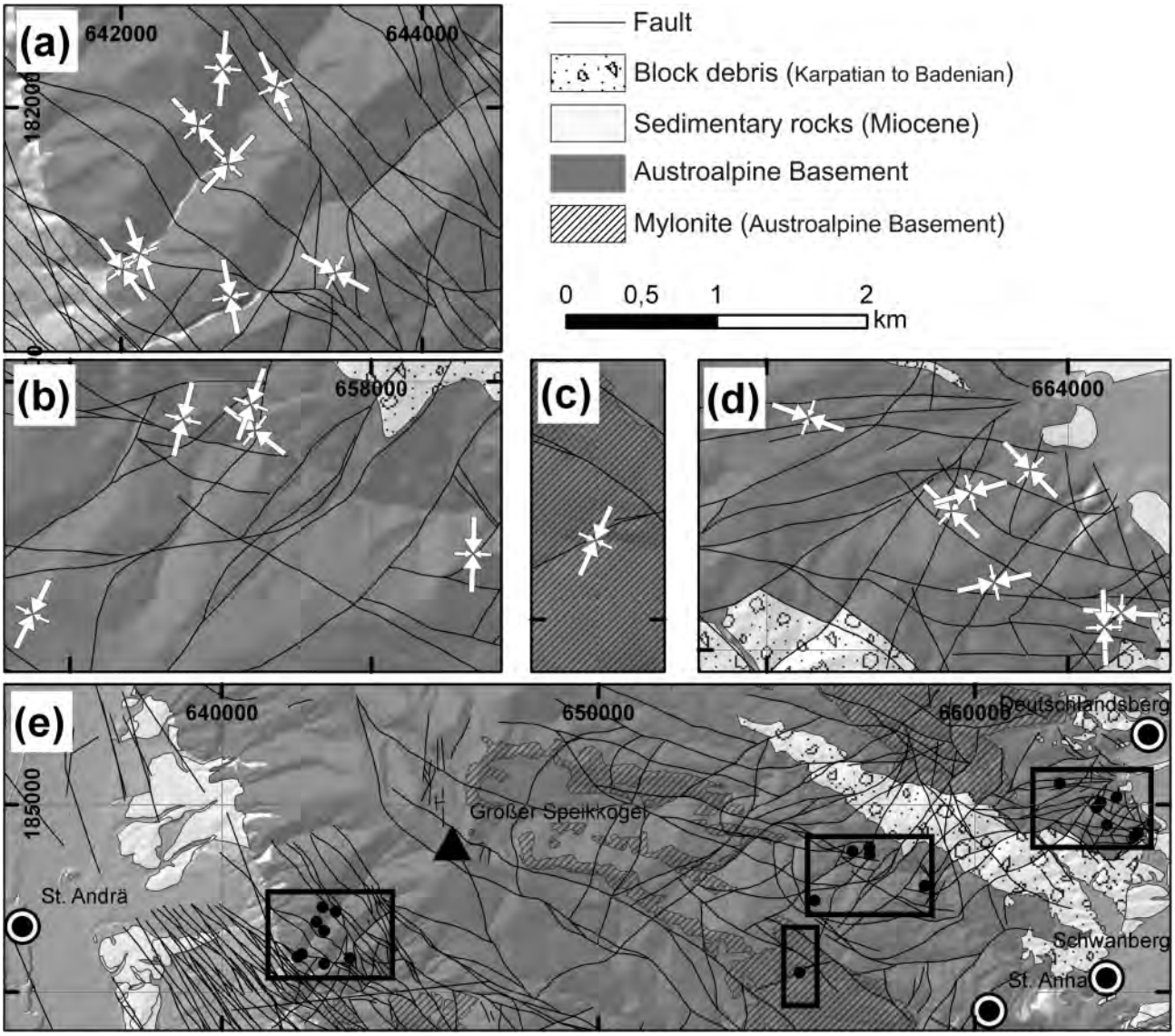

Figure 13: Regional distribution of the paleostress axes with strike slip kinematics. Grid is in Austrian BMN M34 system. 10 m resolution DEM provided by Bundesamt für Eich- und Vermessungswesen (Vienna).

Apart from the methodological problem of discerning and analysing brittle structures in a appropriate way, as well as comparing and (tentatively) fitting new data into an existing framework, at least two questions remain to be addressed:

Is it likely that structural associations of a certain type are generated repeatedly in different subsequent brittle deformation events? Moreover, could this happen irrespectively of the exhumation history (and related changing physical boundary conditions) of the rock mass?

Is it likely that the developed small-scale structures stay preserved, discernable, and are without much influence on the stress orientation next-to-develop; at least at the local scale?

5.1 Comparison/interpretation of data

Clear overprinting relationships, or other decisive markers of age relationships for the brittle small scale structures are rare within the basement rocks of the Koralpe. The few exceptions seem to favour W-E directed extension as a relatively younger discernible brittle deformational event against other structures. Relative timing has to rely on the sedimentary and tectonic history of the surrounding Neogene basins.

In the following the scheme proposed by Pischinger et al. (2008) and outlined in chapter 2 of this paper is used for a comparison with the paleostress orientations determined from the small- to mesoscale structures described above. According to Pischinger et al. (2008), the oldest discernable deformation event D1-1 is characterised by a subhorizontal NNW-SSE directed σ_1 and a subhorizontal WSW-ENE trending σ_3. This indicates a strike-slip displacement regime, which is attributed to Ottnangian to Karpatian age. These orientations are prominently present within the conjugate shear fractures (Fig. 10 b) and the faulting-related secondary fractures (Fig. 10 e) of the present study. Even a considerable portion of the analysed conjugate shear fractures displaying normal kinematics and of the tensional/extensional fractures might be fitted to this stress scheme with respect to σ_3 axes (Fig. 10 a, d). The formation of low-angle shears and of listric normal faults is not likely within this deformation event.

D1-2 is interpreted to represent extension in (N)NE – (S)SW direction with subhorizontal σ_3 and subvertical σ_1 axes, caused by widening perpendicular to the tectonic margins of the extruding wedge of the Eastern Alps (Neubauer et al., 2000; Pischinger et al, 2008). Sedimentation of block debris along WNW-ESE trending faults constrains the timing of this event. According to Nebert (1989) sedimentation of these deposits started during the late Karpatian / early Badenian. Several subsets of the analysed data may be attributed to this event. Within the conjugate fractures only a few data indicate extension in SW-NE direction, which could be associated to the D1-2 event (Fig. 10 a). Further some of the faulting related secondary fractures yield paleostress orientations which could be attributed to this event (Fig. 10 d). However, the more easterly orientation of σ_3 estimates from the conjugate fractures and the secondary fractures hampers a reliable separation from D2 related data. Sets of the tensional/extensional fractures (Fig. 10 g) yielding N-S to NNE-SSW directed extension are probably related to this event. Within the low-angle shears, the respective stress axes orientations are found too (Fig. 10 h). Also the listric normal faults (Fig. 10 i) yield NNW-SSE σ_3 estimates, which are compatible with the D1-2 event.

D2 stands for W-E directed extension, with σ_3 subhorizontally in W-E to WNW-ESE directions respectively. Most of the brittle features documented by Pischinger et al. (2008) are related to this event of probable early Badenian age. This prominent event is also constrained by data from the Pohorje mountains (Fodor et al., 2008), where it was attributed to a much longer period than in the Koralpe region. Within the Pohorje the σ_3 estimates scatter between SW-NE and WNE-ESE,

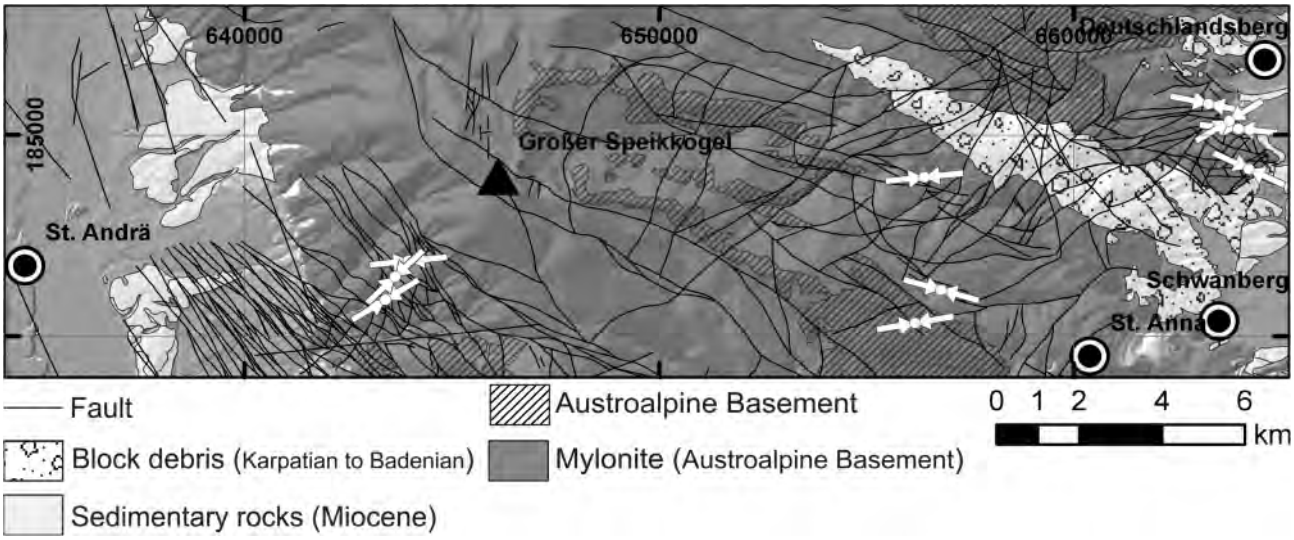

Figure 14: Regional distribution of the paleostress axes with reverse kinematics. Grid is in Austrian BMN M34 system. 10 m resolution DEM provided by Bundesamt für Eich- und Vermessungswesen (Vienna).

which is attributed to spatial variations in the stress field (Fodor et al., 2008).

D2 is clearly reflected in the conjugate fractures data (Fig. 10 a). The major part of fault related secondary fractures and of tensional/extensional fractures also yields similar σ_3 axes (Fig. 10 d, g). This kinematics is also reflected within the low-angle shears (Fig. 10 h) and within single results from the analysis of listric faults (Fig. 10 i).

Deformation phase D3 is subdivided into two simultaneous stages of deformation: D3-1 and D3-2. D3-1 represents a wrench faulting situation with σ1 in NE – SW and σ_3 in SE – NW orientation. According to Pischinger et al. (2008) it is thought to be of middle Badenian to Pannonian age. This is supported by Reischenbacher and Sachsenhofer (2013), who describe faulting of Lower Badenian sediments by D3-1 related faults.

Very few faulting related shears reflect that stress situation. Within the extensional fractures/veins some D3-1 data could be contained within a pronounced cluster of σ_3 data. However, this cluster could also be attributed either to the D2 or D3-2 normal faulting events. The conjugate fractures contain a cluster of strike slip data indicating NNE-SSW compression (mean vector 016/00) relatable to the D3-1 event.

D3-2, thought to be synchronous to D3-1 (Pischinger et al., 2008), is characterised by extension in approximately SE-NW direction. Such synchronous stages of different stress orienta-

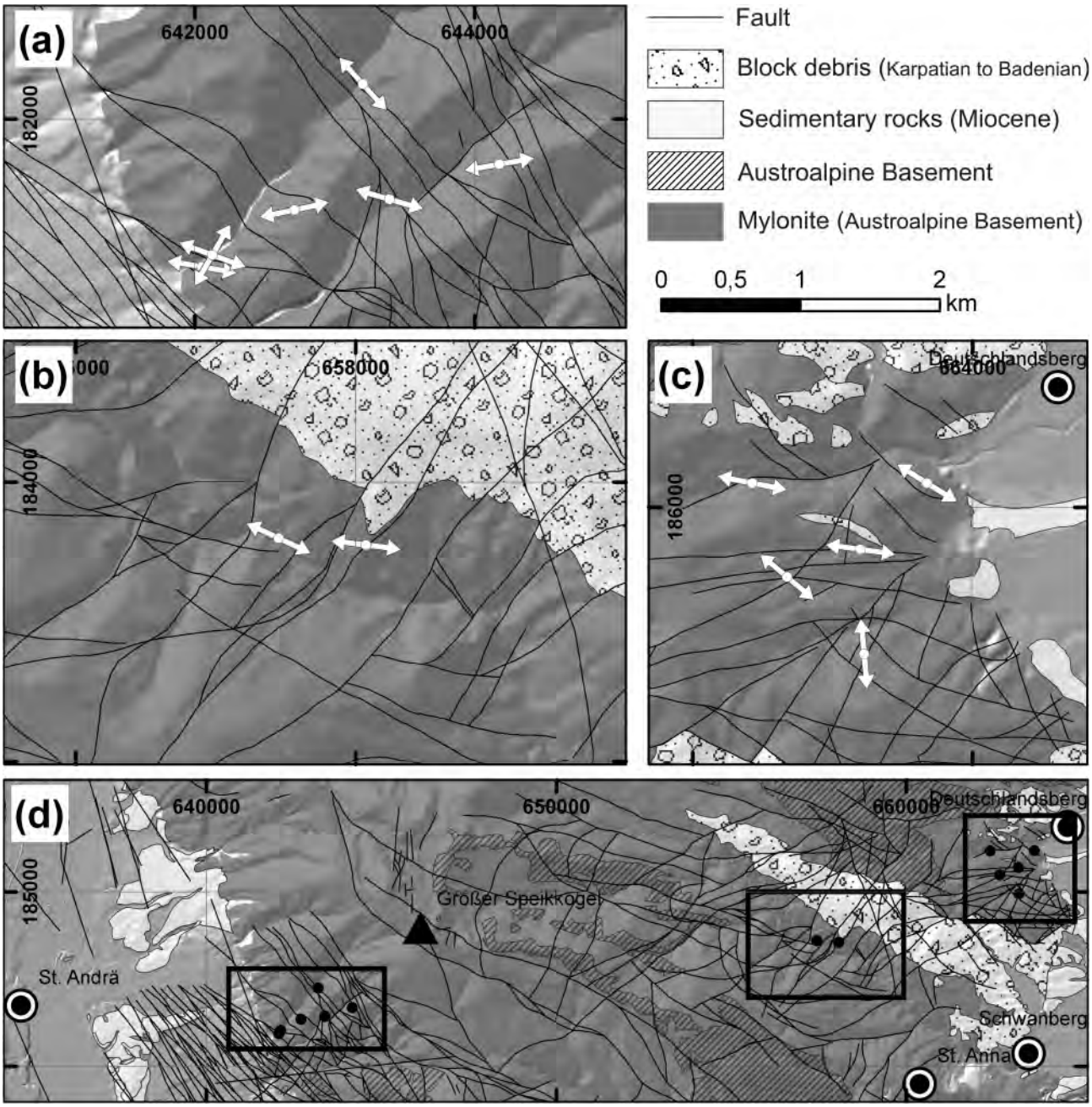

Figure 15: Regional distribution of "extension" axis derived from vein data. Grid is in Austrian BMN M34 system. 10 m resolution DEM provided by Bundesamt für Eich- und Vermessungswesen (Vienna).

tion may be indicative for a transtensional regime, as indicated by Fodor et al (2008) for the Pohorje Mountains.

The low angle shears show a prominent concentration of σ_3 axes (ranges) plunging subhorizontally to NW, while constructed σ_1 plunge steeply (Fig. 10 h). Within the other structural associations only rare data sets with the respective paleostress orientation exist. For the extensional fractures and veins (Fig. 10 g) it seems possible that D3-2 data could be contained in a cluster attributable also to D3-1 and/or D2.

D4, constrained only by a few data sets, is considered to be the result of Pannonian to Pliocene compression in approximately E-W direction (Pischinger et al., 2008; Reischenbacher, 2008, and Reischenbacher and Sachsenhofer, 2013). Accordingly, σ_1 should be found in that direction subhorizontally and σ_3 plunging very steeply to subvertically, thus favouring thrusting-style structural associations.

As for the conjugate fractures, the respective subset represents exclusively that stress situation (Fig. 10 c). In the analysis of faulting-related secondary fractures, that stress orientation is well present, too (Fig. 10 f). However, there is a considerable scatter in the orientation of the constructed stress axes and sub-concentrations of σ_1 axes even in WNW - ESE and WSW - ENE directions appear.

W-E directed compression is a widespread phenomenon within the Eastern Alps (Decker et al., 1993; Nemes et al., 1995; Vrabec and Fodor, 2005), probably related to the slowing down and ceasing subduction of the European plate below the Eastern Carpathians (Peresson and Decker, 1997). Fodor et al. (2008) documented a strike-slip type stress field with a horizontal, NE to E trending σ_1 for the Pohorje mountains, which they associated with a short period around the late Sarmatian and the early Pannonian. Yet, in contrary to the rest of the Pannonian basin (e.g. Fodor et al., 1999), compressional structures are not known from within the Styrian Basin (Wagner, 2010) and time constraints are missing from within the Koralpe range.

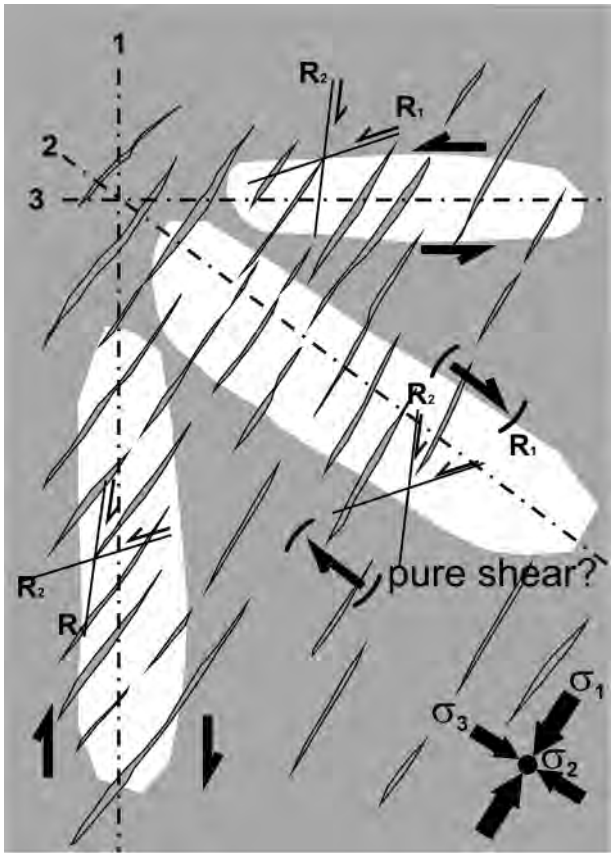

Figure 16: Schematic system of extension veins with σ_1 parallel and σ_3 at right angles to the depicted vein traces. Axis of σ_2 is perpendicular to the plane of the sketch (see lower right corner of figure). Limited exposure is marked by white patches and, if not considered, may result in a biased determination of shear kinematics from different outcrop orientations (dashed lines 1, 2, 3 and blank fields) and an erroneous interpretation.

6. Conclusions

Despite of considerable restraints, the application of subtle geometrical relationships for the analysis of structural associations of brittle character may act as a serious arbitration aid in the interpretation of displacements and derived stresses.

Comparing the findings of the present study with the outcomes of analyses based mainly on fault slip kinematic data (Pischinger et al., 2008, Reischenbacher, 2008, and Reischenbacher and Sachsenhofer, 2013) and, without “forcing” data, we conclude that:

- Map representation of the derived kinematic axes seems crucial to allow a reliable interpretation of the data, as a sole synopsis with the help of stereographic projections may be misleading in terms of the discrimination of different tectonic events.
- The analysed data yield paleostress axes which may be attributed to the three Andersonian fault types.
- The results are similar to the ones achieved by fault slip analysis.
- Yet, a reliable timing of the different tectonic events is not possible on the basis of the structures analysed.
- Time constraints given by the surrounding sedimentary basins are limited by their maximum (Ottnagium and Karpatium) and minimum age (Sarmatian).
- The data attributable to “normal” tectonics can be summarized to three directions of extension (SW-NE, W-E and NNW-SSE). SW-NE directed extension dominates the area near to the Lavanttal fault zone, indicating the opening direction of the Lavanttal Basin. More pronounced scatter of extension direction characterizes the central Koralpe, σ_3 directions indicate W-E, NW-SE and NE-SW extension respectively. W-E directed extension (scattering between WSW-ENE and WNW-ESE) dominates the eastern margin towards the Styrian Basin.
- The “strike slip” data can be summarized to represent two events, with interchanging orientation of the σ_1 and the σ_3 axes. The vicinity of the Lavanttal fault zone is characterized by N-S to NW-SE directed compression axis. N-S to NNE-SSW directed σ_1 dominates the central area of the Koralpe. The eastern margin yields predominating W-E to WNW-ESE directed, and singular N-S directed σ_1 axes.

- Moderate “reverse” tectonics in WSW-ENE to WNW-ESE direction is confirmed. Similar structures have not yet been reported from the Styrian Basin and therefore age constraints are missing. Similarity of σ_1 orientation to some of the strike slip data indicate that they may be related to strike slip tectonics.
- However, not all results of the performed analyses fit into the applied scheme of deformation events.
- Further, the applied scheme only considers the tectonic evolution during the Neogene, although brittle tectonic deformation is also probable for the Paleogene.
- Paleogene tectonics is not recorded by sedimentary basins in the vicinity of the Koralpe and therefore no parallelization between basement and basin tectonics is possible.

Acknowledgements

We thank Mag. Ing. Gerhard Harer (ÖBB Infrastruktur AG) for the permission to use field and tunnel data mapped during site investigation for the Koralm tunnel and during heading of KAT1 tunnel lot for this paper.

Kurt Decker and Lazlo Fodor are thanked for their critical and helpful reviews to improve this paper. The editor Michael Wagreich is thanked for his efforts to bring this work to an end.

References

Anderson, E.M., 1951. The Dynamics of Faulting and Dyke Formation with Applications to Britain. Oliver and Boyd, Edinburgh, 206 pp.

Andeweg, B., 2002. Cenozoic tectonic evolution of the Iberian Peninsula, causes and effects of changing stress fields. PhD Thesis, Vrije Universiteit Amsterdam, Amsterdam, 178 pp.

Angelier, J., 1989. From orientation to magnitudes in paleostress determinations using fault slip data. Journal of Structural Geology, 11, 37 - 50.

Angelier, J., 1994. Fault Slip Analysis and Palaeostress Reconstruction. In: P.L. Hancock (Editor), Continental Deformation. Pergamon Press, Oxford, pp. 53-100.

Bada, G., Horvath, F., Dovenyi, P., Szafian, P. Windhoffer, G. and Cloething, S., 2007. Present-day stress field and tectonic inversion in the Pannonian basin. Global and Planetary Change, 58(1-4), 165-180.

Barron, K., 1971. Brittle fraction initiation in and ultimate failure of rocks; Part III:Anisotriopic rocks:Experimental results. International Journal of Rock Mechanics and Mining Sciences, 8, 565-575.

Beach, A., 1975. The geometry of en-echelon vein arrays. Tectonophysics, 28, 245-263.

Becker, L.P., 1979. Geologische Karte der Republik Österreich 1:50.000 - 162 Köflach. Geologische Bundesanstalt, Wien.

Beck-Mannagetta, P., 1952. Zur Geologie und Paläontologie des Tertiärs des unteren Lavanttales. Jahrbuch der Geologischen Bundesanstalt, 95, 1-102.

Beck-Mannagetta, P., 1980. Geologische Karte der Republik Österreich 1:50.000 - 188 Wolfsberg. Geologische Bundesanstalt, Wien.

Beck-Mannagetta, P., Eisenhut, M., Ertl, V. and Homann, O., 1991. Geologische Karte der Republik Österreich 1:50.000 - 189 Deutschlandsberg. Geologische Bundesanstalt, Wien.

Beck-Mannagetta, P. and Stingl, K., 2002. Geologische Karte der Republik Österreich 1:50.000 - 206 Eibiswald. Geologische Bundesanstalt, Wien.

Blenkinsop, T.G., 2008. Relationships between faults, extension fractures and veins, and stress. Journal of Structural Geology, 30, 622-632.

Bons, P.D., Elburg, M.A. and Gomez-Rivas, E., 2012. A review of the formation of tectonic veins and their microstructures. Journal of Structural Geology, 43: 33-62.

Bott, M.H.P., 1959. The mechanics of oblique slip faulting. Geological Magazine, 96, 109-117.

Bradshaw, G.A. and Zoback, M.D., 1988. Listric normal faulting, stress refraction, and the state of stress in the Gulf Coast basin. Geology, 16, 271-274.

Brosch, F.J., Schachner, K., Blumel, M., Fasching, A. and Fritz, H., 2000. Preliminary investigation results on fabrics and related physical properties of an anisotropic gneiss. Journal of Structural Geology, 22, 1773-1787.

Celerier, B., 1999. FSA.18: Fault Slip Analysis Software. http://www.isteem.univ-montp2.fr/PERSO/celerier/software/fsa18.html.

Coelho, S., Passchier, C. and Marques, F., 2006. Riedel-shear control on the development of pennant veins: field example and analogue modelling. Journal of Structural Geology, 28, 1658-1669.

Decker, K., Meschede, M. and Ring, U., 1993. Fault slip analysis along the northern margin of the Eastern Alps (Molasse, Helvetic nappes, North and South Penninic flysch, and the Northern Calcareous Alps). Tectonophysics, 223, 291-312.

Doblas, M., 1998. Slickenside kinematic indicators. Tectonophysics, 295, 187-197.

Doblas, M., Mahecha, V., Hoyos, M. and Lopez-Ruiz, J., 1997. Slickenside and fault surface kinematic indicators on active normal faults of the Alpine Betic Cordilleras, Granada, southern Spain. Journal of Structural Geology, 19, 159-170.

Donath, F.A., 1961. Experimental study of shear failure in anisotropic rocks. Geological Society of America Bulletin, 72, 985-990.

Dula, W.F., 1991. Geometric models of listric normal faults and rollover folds. American Association of Petroleum Geologists Bulletin, 75, 1609-625.

Dunkl, I., Kuhlemann, J., Reinecker, J. and Frisch, W., 2005. Cenozoic relief evolution of the Eastern Alps – constraints from apatite fission track age-provenance of Neogene intramontane sediments. Austrian Journal of Earth Sciences, 98: 92-105.

Dunne, W. M., Hancock, P.M. 1994. Paleostress analysis of small scale brittle structures. In: Hancock, P. L., Continental deformation. Pergamon Press, pp. 101-120.

Ebner, F. and Rantitsch, G., 2000. Das Gosaubecken von Kainach - ein Überblick. Mitteilungen der Gesellschaft der Geologie und Bergbaustudenten in Österreich, 44, 157-172.

Ellis, P.G. and McClay, K.R., 2007. Listric extensional fault systems – results of analogue model experiments. Basin Research, 1, 55-70.

Egger, H. Krenmayr, H.-G., Mandl, G.W., Matura, A., Nowotny, G., Pascher, G., Pestal, G., Pistotnik, J., Rockenschaub, M., Schnabel, W., 1999. Geologische Übersichtskarte der Republik Österreich 1:1500 000. Geologische Bundesanstalt, Wien.

Engelder, J.T. and Scholz, C.H., 1976. The role of asperity indentation and ploughing in rock friction, 2: Influence of relative hardness and normal load. International Journal of Rock Mechanics and Mining Sciences, 13, 155-163.

Engelder, T. and Geiser, P., 1980. On the use of regional joint sets as trajectories of paleostress fields during the development of the Appalachian Plateau, New York. Journal of Geophysical Research, 85, 6319-6341.

Etchecopar. A., Vasseur, G. ,Daignieres, M., 1981. An inverse problem in microtectonics for the determination of stress tensors from fault striation analysis. Journal of Structural Geology, 3, 51-65.

Fodor, L., Csontos, L., Bada, G., Györfi, I. and Benkovics, L., 1999. Tertiary tectonic evolution of the Pannonian Basin system and neighbouring orogens: a new synthesis of palaeostress data. In: B. Durand, L. Jolivet, F. Horváth and M. Seranne (eds.), The Mediterranean Basins: Tertiary Extension within the Alpine Orogen. Geological Society Special Publications, Geological Society, London, pp. 295-334.

Fodor, L., Gerdes, A., Dunkl, I., Koroknai, B., Pécskay, Z., Trajanova, M., Horváth, P., Vrabec, M., Jelen, B., Balogh, K., Frisch, W., 2008. Miocene emplacement and rapid cooling of the Pohorje pluton at the Alpine-Pannonian-Dinaridic junction, Slovenia. Swiss Journal of Geosciences, 101, 255-271.

Fossen, H., 2010. Structural Geology. Cambridge University Press, Cambridge, 480 pp.

Fleuty, M.J. and Weaver, J.D., 1975. Slickensides and slickenlines. Geological Magazine, 112, 319-322.

Fry, N., 1999. Striated faults: visual appreciation of their constraint on possible paleostress tensors. Journal of Structural Geology, 21, 7-21.

Ghisetti, F., 2000. Slip partitioning and deformation cycles close to major faults in southern California: Evidence from small-scale faults. Tectonics, 19, 25-43.

Gomez-Rivas, E. and Griera, A., 2012. Shear fractures in anisotropic ductile materials: An experimental approach. Journal of Structural Geology, 34, 61-76.

Goodman, R.E., 1976. Methods of geological engineering in discontinuous rock. West Publishing Co., St. Paul MN, 472 pp.

Goodman, R.E., 1989. Introduction to Rock Mechanics. Wiley, 562 pp.

Goricki, A. and Harer, G., 2004. Spannungsmessung für das Projekt Koralmtunnel - Methoden, Ergebnisse, Diskussion. In: R. Poisel and E. Tentschert (Editors), 2nd Coll. Rockmech. - Theory and Practice. Mitteilungen für Ingenieurgeologie und Geomechanik Band 6, pp. 55-65.

Hancock, P.L., 1985. Brittle microtectonics: principles and practice. Journal of Structural Geology, 7, 437-457.

Hancock, P. L., Al-Khadi, A., Barka, A. A. and Bevan, T. G., 1987. Aspects of analysing brittle structures. Annales Tectonicae, 1, 5-19.

Healy, D., Jones, R. R. and Holdsworth, R.E., 2006. Three-dimensional brittle shear fracturing by tensile crack interaction. Nature, 439, 64-67.

Hejl, E., 1997. 'Cold spots' during the Cenozoic evolution of the Eastern Alps: thermochronological interpretation of apatite fission-track data. Tectonophysics, 272, 159-173.

Hejl, E., 1998. Über die känozoische Abkühlung und Denudation der Zentralalpen östlich der Hohen Tauern - Apatit-Spaltspuranalyse. Mitteilungen der Österreichischen Geologischen Gesellschaft, 89, 179-199.

Jaeger, J.C., 1959. The frictional properties of joints in rock. Pure and Applied Geophysics, pp. 148-158.

Jaeger, J. C. 1960. Shear Failure of Anistropic Rocks. Geological Magazine, 97, 65-72.

Jaeger, J. C. and Cook, N.G.W., 1979. Fundamentals of Rock Mechanics. Chapman & Hall, London, 593 pp.

Joanneum Research and GIS-STMK, 1999. Provisorische Geologische Karte der Republik Österreich 1:50.000 - 161 Knittelfeld. Geologische Bundesanstalt, Wien.

John, K.W. and Deutsch, R., 1974. Die Anwendung der Lagenkugel in der Geotechnik. In: E. Fecker, H.-P. Gotz, G. Sauer and G. Spaun (Editors), Festschrift; Leopold Mueller-Salzburg zum 65. Geburtstag. Privately published, Karlsruhe, Federal Republic of Germany (DEU), Karlsruhe, pp. 137-159.

Krantz, R.W., 1988. Multiple fault sets and three-dimensional strain: Theory and application. Journal of Structural Geology, 10, 225-237.

Kröll, 1988. Steirisches Becken-Südburgenländische Schwelle - Reliefkarte des prätertiären Untergrundes. Geologische Bundesanstalt, Wien.

Kurz, W., Fritz, H., Tenczer, V. and Unzog, W., 2002. Tectonometamorphic evolution of the Koralm Complex (Eastern Alps): constraints from microstructures and textures of the 'Plattengneis' shear zone. Journal of Structural Geology, 24, 1957-1970.

Kurz, W. and Fritz, H., 2003. Tectonometamorphic Evolution of the Austroalpine Nappe Complex in the Central Eastern Alps—Consequences for the Eo-Alpine Evolution of the Eastern Alps. International Geology Review, 45(12): 1100-1127.

Kurz, W., Wölfler, A., Rabitsch, R. and Genser, J., 2011. Polyphase movement on the Lavanttal Fault Zone (Eastern Alps): reconciling the evidence from different geochronological indicators. Swiss Journal of Geosciences, 104, 323-343.

Lajtai, E.Z. and Lajtai, V.N., 1974. The evolution of brittle fracture in rocks. Journal of the Geological Society, 130, 1-16.

Lisle, R.J., 1989. A simple construction for shear stress. Journal of Structural Geology, 11, 493-495.

Lisle, R.J. and Leyshon, P.R., 2004. Stereographic Projection Techniques for Geologists and Civil Engineers. Cambridge University Press, Cambridge, 112 pp.

Lopes Cardozo, G.G.O. and Behrmann, J.H., 2006. Kinematic analysis of the Upper Rhine Graben boundary fault system. Journal of Structural Geology, 28, 1028-1039.

Logan, J.M., Friedman, M., Higgs, N., Dengo, C. and Shimamoto, T., 1979. Experimental studies of simulated gouge and their application to studies of natural zones. US Geological Survey, Open-file Report 791239, 305-343.

Mandl, G., 1987. Discontinuous fault zones. Journal of Structural Geology, 9, 105-110.

Mandl, G., 1988. Mechanics of tectonic faulting - models and basic concepts. Developments in structural geology. Elsevier, Amsterdam, 407 pp.

Mandl, G., 2000. Faulting in brittle rocks. Springer, Berlin, 434 pp.

Mandl, G., 2005. Rock joints- the mechanical genesis. Springer, Berlin, 221 pp.

Marrett, R., Allmendinger, R. W., 1990. Kinematic analysis of fault-slip data. Journal of Structural Geology, 12, 973.986.

Meschede, M., 1994. Methoden der Strukturgeologie. Enke, Stuttgart, 169 pp.

Moore, D.E., Summers, R. and Byerlee, J.D., 1989. Sliding behavior and deformation textures of heated illite gouge. Journal of Structural Geology, 11, 329-342.

Nebert, K., 1989. Das Neogen zwischen Sulm und Lassnitz (Suedweststeiermark). Jahrbuch der Geologischen Bundesanstalt Wien, 132, 727-743.

Nemes, F., Pavlik, W. and Moser, M., 1995. Geologie und Tektonik im Salzatal (Steiermark) – Kinematik und Paläospannungen entlang des Ennstal-Mariazell-Blattverschiebungssystems in den Nördlichen Kalkalpen. Jahrbuch der Geologischen Bundesanstalt, 138, 349-367.

Nemes, F., Neubauer, F., Cloetingh, S. and Genser, J., 1997. The Klagenfurt Basin in the Eastern Alps: an intra-orogenic decoupled flexural basin? Tectonophysics, 282, 189-203.

Neubauer, F., 1991. Kinematic indicators in the Koralm and Saualm eclogites (Eastern Alps). Zentralblatt für Mineralogie, Geologie und Paläontologie, Teil I: Allgemeine, Angewandte, Regionale und Historische Geologie, 1, 139-155.

Neubauer, F., Fritz, H., Genser, J., Kurz, W., Nemes, F., Wallbrecher, E., Wang, X. and Willingshofer, E., 2000. Structural evolution within an extruding block: model and application to the Alpine-Pannonian system. In: F.K. Lehner and J.L. Urai (eds.), Aspects of tectonic faulting. Festschrift in honour of Georg Mandl. Springer, Berlin, pp. 141-153.

Olson, J. E. and Pollard, D. D., 1991. The initiation and growth of en echelon veins. Journal of Structural Geology, 13, 595-608.

Ortner, H., Reiter, F. and Acs, P., 2002. Easy handling of tectonic data: the programs TectonicVB for Mac and TectonicsFP for Windows™. Computers & Geosciences, 28, 1193-1200.

Oncken, O., 1988. Aspects of the reconstruction of the stress history of a fold and thrust belt (Rhenish Massif, Federal Republic of Germany). Tectonophysics, 152, 19-40.

Patalakha, Y., 1986. The problem of listric faults. International Geological Review, 28, 1416-422.

Peacock, D. C. P. and Sanderson, D.J., 1992. Effects of layering and anisotropy on fault geometry. Journal of the Geological Society, 149, 793-802.

Peresson, H. and Decker, K., 1996. From extension to compression: Late Miocene stress inversion in the Alpine-Carpathian-Pannonian transition area. Mitteilungen der Gesellschaft der Geologie und Bergbaustudenten in Österreich, 41: 75-86.

Peresson, H. and Decker, K., 1997. Far-field effects of Late Miocene subduction in the Eastern Carpathians: E-W compression and inversion of structures in the Alpine-Carpathian-Pannonian region. Tectonics, 16, 38-56.

Petit, J.P., 1987. Criteria for the sense of movement on fault surfaces in brittle rocks. Journal of Structural Geology, 9, 597-608.

Petit, J.-P., Auzias, V., Rawnsley, K. and Rives, T., 2000. Development of joint sets in the vicinity of faults. In: Lehner, F. K. & Urai, J. L. (eds.), Aspects of tectonic faulting. Festschrift in honour of Georg Mandl. Springer, Berlin, pp. 167-183.

Piller, W.E. et al., 2004. Die Stratigraphische Tabelle von Österreich 2004 (sedimentäre Schichtfolgen). Österreichische stratigraphische Kommission und Kommission für die paläontologische und stratigraphische Erforschung Österreichs der Österreichischen Akademie der Wissenschaften.

Pischinger, G., Kurz, W., Übleis, M., Egger, M., Fritz, H., Brosch, F.J. and Stingl, K., 2008. Fault slip analysis in the Koralm Massif (Eastern Alps) and consequences for the final uplift of “cold spots” in Miocene times. Swiss Journal of Geosciences, 101, 235-254.

Pollard, D.D. and Aydin, A., 1988. Progress in understanding jointing over the past century. Geological Society of America Bulletin, 100, 1181-1204.

Popotnig, A., Decker, K. and Grasemann, B., 2007. Active kinematics and tectonic geomorphology of the Lavanttal Fault. Geophysical Research Abstracts, 9(A-03270).

Price, N. J. and Cosgrove, J. W., 1990. Analysis of geological structures. Cambridge University Press, Cambridge, 502 pp.

Priest, S. D., 1985. Hemispherical Projection Methods in Rock Mechanics. George Allen & Unwin, London, 124 pp.

Priest, S. D., 1993. Discontinuity Analyses for Rock Engineering. Chapman & Hall, London, 473 pp.

Putz, M., Stüwe, K., Jessell, M. and Calcagno, P., 2006. Three-dimensional model and late stage warping of the Plattengneis Shear Zone in the Eastern Alps. Tectonophysics, 412, 87-103.

Quade, H., 1984. Die Lagenkugelprojektion in der Tektonik – Das SCHMIDTsche Netz und seine Anwendung. Clausthaler Tektonisch Hefte, 20, Ellen Pilger Verlag, Clausthal-Zellerfeld, 197 pp.

Ragan, D. M, 2009. Structural Geology: An Introduction to Geometrical Techniques. Cambridge University Press, 624 pp.

Ramsay, J.G. and Huber, M.I., 1987. The Techniques of Modern Structural Geology. Volume 2: Folds and Fractures, 2. Academic Press, London, pp. 309-700.

Ratschbacher, L., Frisch, W., Linzer, H.-G. and Merle, O., 1991. Lateral extrusion in the Eastern Alps, part 2: structural analysis. Tectonics, 10, 257-271.

Rawnsley, K. D., Rives, T., Petit, J.-P., Hencher, S.R. and Lumsden, A.C., 1992. Joint perturbations at faults. Journal of Structural Geology ,14, 939-951.

Reches, Z., 1978. Analysis of faulting in a three-dimensional strain field. Tectonophysics, 47, 109-129.

Reches, Z. and Dietrich, J.H., 1983. Failure of rock in three dimensional strain fields. I: Failure of rock in polyaxial, servo-controlled experiments. Tectonophysics, 95,111– 32.

Reches, Z. and Lockner, D.A., 1994. Nucleation and growth of faults in brittle rocks. Journal of Geophysical Research, 99, 18159-8174.

Reinecker, J. and Lenhardt, W.A., 1999. Present-day stress field and deformation in eastern Austria. International Journal of Earth Sciences, 88, 532-550.

Reischenbacher, D., 2008. Beckenentwicklung und Bildung von Kohleflözen und organisch-reichen Sedimenten am Beispiel des neogenen Lavanttaler Beckens. PhD Thesis, Montanuniversität Leoben, Leoben, 295 pp.

Reischenbacher, D. and Sachsenhofer, R., 2013. Basin formation during the post-collisional evolution of the Eastern Alps: the example of the Lavanttal Basin. International Journal of Earth Sciences, 102, 517-543.

Reiter, F. and Acs, P., 1996-2007. TectonicsFP - Computer Software for Structural Geology, Innsbruck.

Riedel, W. 1929. Zur Mechanik geologischer Brucherscheinungen. Ein Beitrag zum Problem der „Fiederspalten“. Zentralblatt für Mineralogie, Geologie und Paläontologie, Abteilung B, 354-368.

Scheidegger A.E., 1980. Alpine joints and valleys in the light of the neotectonic stress field. Rock Mechanics, 9, 109–124.

Scheidegger, A.E. 2001. Surface joint systems, tectonic stresses and geomorphology: a reconciliation of conflicting observations. Geomorphology, 38, 213-219.

Scholz, C.H. and Engelder, J.T., 1976. The role of asperity indentation and ploughing in rock friction, 1: Asperity creep and stickslip. International Journal of Rock Mechanics and Mining Sciences, 13, 149-154.

Schrader, F., 1994. Die eingeschränkte Gültigkeit des BOTTschen Postulats und Konsequenzen für die Harnischanalyse. Göttinger Arbeiten zur Geologie und Paläontologie, Sb1, (5. Symp.TSK), 7-9.

Schrader, F., 1999. Do foliation surfaces and "stretching" lineations represent XY resp. X of finite strain? Göttinger Arbeiten zur Geologie und Paläontologie, Sb4, 173-174.

Skempton, A.W., 1966. Some observations on tectonic shear zones. Proceedings 1st ISRM Congress. International Society for Rock Mechanics, Lisbon, pp. 329-335.

Srivastava, D.C., 2000. Geometrical classification of conjugate vein arrays. Journal of Structural Geology, 22, 713-722.

Strauss, P., Wagreich, M., Decker, K. and Sachsenhofer, R., 2001. Tectonics and sedimentation in the Fohnsdorf-Seckau Basin (Miocene, Austria): from a pull-apart basin to a half-graben. International Journal of Earth Sciences, 90, 549-559.

Tang, C. And Hudson, J.A. 2010. Rock Failure Mechanisms-Explained and Illustrated. CRC Press, Boca Raton, FL, 364 pp.

Thiedig, F. and Weissenbach, N., 1975. Die junge Bruchtektonik im Bereich der Saualpe. Clausthaler geologische Abhandlungen, 1, pp. 155-174.

Treagus, S.H., 1986. Some applications of the Mohr diagram for three-dimensional strain. Journal of Structural Geology, 8, 819-830.

Twiss, R.J. and Moores, E.M., 2007. Structural Geology. W.H. Freeman and Company, New York, 736 pp.

Vanek, R., Pischinger, G. and Brosch, F.J., 2001. Kinematic Discontinuity Analysis. Felsbau, 19, 31-36.

Vrabec, M. and Fodor, L., 2005. Late Cenozoic tectonics of Slovenia: Structural styles at the northeastern corner of the Adriatic microplate. In: N. Pinter, G. Grenerczy, J. Weber and D. Medak (Editors), Proceedings of the NATO Advanced Research Workshop on The Adria Microplate: GPS Geodesy, Active Tectonics and Hazards. IV. Earth and Environmental Sciences. Springer, Veszprem, Hungary, pp. 151-168.

Wagner, T., 2010. Young uplift in the non-glaciated parts of the Eastern Alps - geomorphological and geochronological constraints. PhD Thesis, Karl-Franzens University, Graz, 162 pp.

Wallbrecher, E., 1986. Tektonische und gefügekundliche Arbeitsweisen. Enke, Stuttgart, 244 pp.

Weissenbach, N., 1978a. Geologische Karte der Saulpe, Nord (Kärnten) 1:25.000. Geologische Bundesanstalt, Wien.

Weissenbach, N., 1978b. Geologische Karte der Saulpe, Süd (Kärnten) 1:25.000. Geologische Bundesanstalt, Wien.

Wyllie, D.C. and Mah, C.W., 2004. Rock Slope Engineering. Civil and Mining. Spon Press, New York, 456 pp.

Wölfler, A., Kurz, W., Fritz, H. and Stüwe, K., 2011. Lateral extrusion in the Eastern Alps revisited: Refining the model by thermochronological, sedimentary, and seismic data. Tectonics, 30(4): TC4006.

Received: 18 Juny 2012
Accepted: 25 March 2014

Franz-Josef BROSCH[1)] & Gerald PISCHINGER[1)2)*)]

[1)] Institute of Applied Geosciences, TU Graz, Rechbauerstraße 12, A-8010 Graz, Austria;

[2)] Geoconsult ZT GmbH, Hölzlstraße 5, A-5071 Wals bei Salzburg, Austria;

[*)] Corresponding author, gerald.pischinger@tugraz.at